Seasonal versus synoptic variability in planktonic production in a high-latitude marginal sea: The Gulf of St. Lawrence (Canada)

V. Le Fouest, Bruno Zakardjian, Francois J. Saucier, Michel Starr

Seasonal versus synoptic variability in planktonic production in a high-latitude marginal sea: The Gulf of St. Lawrence (Canada)

V. Le Fouest, B. Zakardjian, and F. J. Saucier
Institut des Sciences de la Mer de Rimouski (ISMER), Université du Québec à Rimouski, Rimouski, Quebec, Canada

M. Starr
Fisheries and Oceans Canada, Maurice Lamontagne Institute, Mont-Joli, Quebec, Canada

Received 8 April 2004; revised 16 November 2004; accepted 4 May 2005; published 21 September 2005.

[1] The Gulf of St. Lawrence (Canada) is a subarctic marginal sea characterized by highly variable hydrodynamic conditions that generate a spatial heterogeneity in the marine production. A better understanding of physical-biological linkages is needed to improve our ability to evaluate the effects of climate variability and change on the gulf's planktonic production. We develop a three-dimensional (3-D) eddy permitting resolution physical-biological coupled model of plankton dynamics in the Gulf of St. Lawrence. The planktonic ecosystem model accounts for the competition between simplified herbivorous and microbial food webs that characterize bloom and post-bloom conditions, respectively, as generally observed in temperate and subarctic coastal waters. It is driven by a fully prognostic 3-D sea ice-ocean model with realistic tidal, atmospheric, and hydrological forcing. The simulation shows a consistent seasonal primary production cycle, and highlights the importance of local sea ice dynamics for the timing of the vernal bloom and the strong influence of the mesoscale circulation on planktonic production patterns at subregional scales.

Citation: Le Fouest, V., B. Zakardjian, F. J. Saucier, and M. Starr (2005), Seasonal versus synoptic variability in planktonic production in a high-latitude marginal sea: The Gulf of St. Lawrence (Canada), *J. Geophys. Res.*, *110*, C09012, doi:10.1029/2004JC002423.

1. Introduction

[2] General circulation models generally predict that global climate change associated with increased greenhouse gas concentrations in the atmosphere will lead to an amplified warming in the Arctic and its adjacent seas over the next century (5°–8°C in 2070 [e.g., *Holland and Bitz*, 2003]). Among those, the Gulf of St. Lawrence (GSL) is a large semi-enclosed sea of 226,000 km^2 that connects the Great Lakes and the St. Lawrence river with the North Atlantic Ocean [e.g., *Koutitonsky and Budgen*, 1991]. Runoff from the St. Lawrence watershed is the second most important source of freshwater from North America into the North Atlantic Ocean [e.g., *Bourgault and Koutitonsky*, 1999]. The GSL exhibits a subarctic climate with a seasonal sea ice cover present between January and April, and sheds the southernmost extent of sea ice in the Northern Hemisphere. Freshwater runoff, large to moderate tides, and highly synoptic winds drive the gulf's circulation. These physical forcings, coupled with the relatively large dimensions of the gulf (several internal Rossby deformation radii) and an average depth of 150 m, generate a complex hydrodynamics with eddies, coastal upwellings, and fronts superimposed on a mean estuarine-like circulation [e.g., *Koutitonsky and Budgen*, 1991; *Saucier et al.*, 2003]. These hydrodynamic conditions have been shown to have a marked effect on summer primary production in the northwestern Gulf [*Levasseur et al.*, 1992; *Fuentes-Yaco et al.*, 1995, 1996, 1997a, 1997b; *Tremblay et al.*, 1997], and are thought to generate a spatial heterogeneity in the marine production of the GSL [e.g., *de Lafontaine et al.*, 1991]. *Savenkoff et al.* [2001] also suggest that the GSL can be subdivided into distinct subregions on the basis of specific hydrodynamic regimes that affect the nutrient transport and the resulting planktonic production. Recent observations confirm that the high interannual variability in plankton biomass in the Lower Estuary [*Starr and Harvey*, 2000; *Starr et al.*, 2001], the recruitment of fish stocks in the southern gulf [*Runge et al.*, 1999], the aggregation of krill and whales at the head of the Laurentian Channel [*Simard and Lavoie*, 1999; *Lavoie et al.*, 2000], and the water masses properties of the GSL [*Saucier et al.*, 2003] are strongly linked to the influence of climate and freshwater inputs on the mixing and circulation processes. However, it has not yet been possible to quantify together the detailed circulation and the response of the planktonic ecosystem.

[3] Prior to any attempt to predict the effects of global climate variability and change on the GSL system, we must first acquire a better knowledge of the links between the physical environment and the short-term to interannual variations in planktonic production. In order to improve

0148-0227/05/2004JC002423

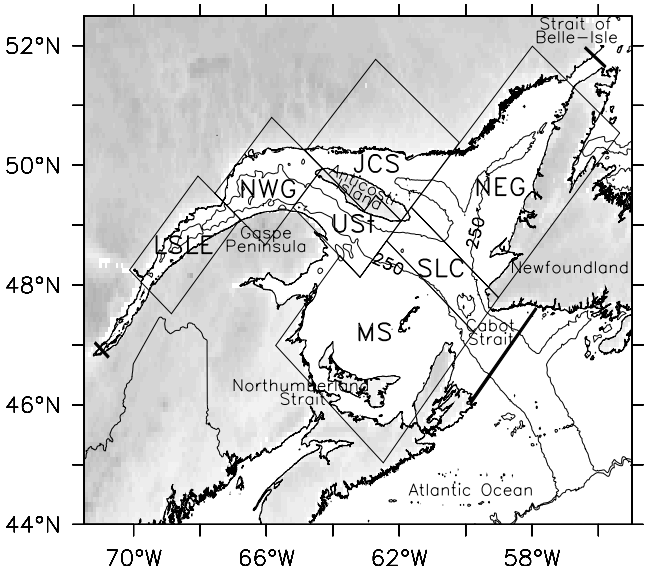

Figure 1. Map of the Estuary and Gulf of St. Lawrence. Thick lines delimit the numerical domain. Boxes indicate the studied subregions: Lower St. Lawrence Estuary (LSLE), northwestern Gulf of St. Lawrence (NWG), Unguedo Strait (USt), Magdalen Shallow (MS), southern Laurentian Channel (SLC), northeastern Gulf of St. Lawrence (NEG), and Jacques Cartier Strait (JCS).

our capability to predict these responses, we need to develop models that reproduce the spatiotemporal variability of the primary and secondary production cycles. Modeling of planktonic production in the St. Lawrence marine system has been limited to one-dimensional (1-D) models of the carbon cycle in the northwestern [*Tian et al.*, 2000] and northeastern [*Tian et al.*, 2001] GSL, to a 2-D modeling study of the phytoplankton production in the Lower Estuary [*Zakardjian et al.*, 2000], and to 3-D modeling of copepods population dynamics [*Zakardjian et al.*, 2003]. This paper aims at describing and quantifying the circulation-planktonic production coupling in the GSL using a detailed 3-D physical-biological model. The coupled model includes both simplified herbivorous and microbial food webs typical of bloom and post-bloom conditions, respectively, as generally observed in temperate and subarctic coastal waters. It is driven by a 3-D high resolution primitive equations ocean-sea ice regional model [*Saucier et al.*, 2003] with realistic tidal, atmospheric, and hydrologic forcing.

[4] In the present paper, we focus on the ecological robustness of the coupled model performances at the regional scale and the subregional variability of the seasonal plankton cycle in response to varied hydrodynamic conditions. These first results demonstrate that the coupled model predicts realistic levels of biomass and a seasonal cycle of planktonic production dominated by the spring phytoplankton bloom, as observed in the GSL. In addition, the model generates a large synoptic and spatial variability in planktonic production in response to the buoyancy-driven circulation, tidal mixing, and wind events. As a consequence, primary production can locally be as important as during the spring bloom. The physical and planktonic ecosystem models are described in section 2, and the results of a simulation presented in section 3. In section 4 we discuss the capabilities and limitations of the coupled model to finally conclude in section 5.

2. Model Formulation

2.1. The 3-D Regional Circulation Model

[5] A detailed description of the deterministic sea ice-ocean coupled model is presented by *Saucier et al.* [2003], and the characteristics are briefly reviewed here. The ocean model is governed by the shallow water equations solved by a finite difference scheme. It incorporates a level 2.5 turbulent kinetic energy equation [*Mellor and Yamada*, 1974, 1982] and diagnostic master length scales. A thermodynamic and dynamic sea ice model [*Semtner*, 1976; *Flato*, 1993] is coupled with the ocean model. Bulk aerodynamic exchange formulas govern the heat and momentum fluxes between the ocean, sea ice, and atmosphere. The model domain covers the Estuary and the Gulf of St. Lawrence and is delimited by three open boundaries at the Cabot Strait, the Strait of Belle-Isle, and the upper limit of the tidal influence near Montreal (Figure 1). The grid resolution is 5 km on the horizontal and ranges from 5 to 20 m in the vertical, with free surface and bottom layers adjusted to topography. The model is fully deterministic and tracer conserving [e.g., *Saucier et al.*, 2003], driven by a detailed atmospheric forcing (3-hourly winds, light, precipitation), daily river runoff data from the St. Lawrence River and the 28 most important tributaries, hourly water levels (co-oscillating tides), and monthly mean temperature and salinity profiles at the Strait of Belle-Isle and Cabot Strait. The model accounts for the variations of sea ice, tides, momentum, heat and salt fluxes, and river discharges with a time step of 300 s and reproduces the high frequency to interannual variations of the circulation, water mass properties, and sea ice cover. Simulations for 1996–1997 [*Saucier et al.*, 2003] and recently through 2003 (F. J. Saucier et al., manuscript in preparation, 2005) have been successfully compared to temperature and salinity data, the sea ice cover, water levels, and past analyses of transport in the Lower Estuary and GSL. In particular, the model reproduces the main well-known circulation features and their seasonal variations. Those include the year-round cyclonic gyre over the northwestern GSL known as the Anticosti Gyre, the Gaspe Current, an unstable buoyancy-driven baroclinic coastal jet, and the southeastward outflow through western Cabot Strait.

2.2. The Planktonic Ecosystem Model

[6] The planktonic ecosystem model (Figure 2) was developed in a moderately complex way in order to limit the number of transfer functions and parameters, and to allow an easier interpretation of the biological response to the high frequency to seasonal variations of environmental conditions generated by the physical model. Primary producers are size-fractionated into large (>5 μm) and small (<5 μm) phytoplankton (LP and SP, respectively) both growing on nitrate (NO3) and ammonium (NH4). Similarly, the secondary producers are divided in mesozooplankton (200–2000 μm, MEZ) and microzooplankton (20–200 μm, MIZ). Two detrital compartments close the cycling of nitrogen, namely particulate and dissolved

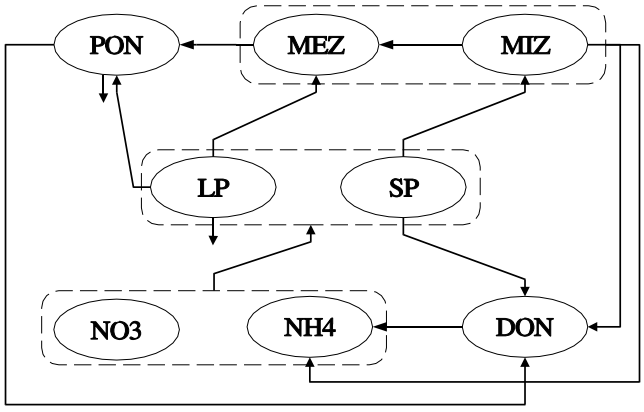

Figure 2. Conceptual planktonic ecosystem model including nitrate (NO3), ammonium (NH4), large phytoplankton (LP), small phytoplankton (SP), mesozooplankton (MEZ), microzooplankton (MIZ), particulate organic nitrogen (PON), and dissolved organic nitrogen (DON). Arrows represent nitrogen fluxes between the biological components.

organic nitrogen (PON and DON, respectively). A close coupling between small phytoplankton and microzooplankton dynamics, autochthonous nitrogen release and DON ammonification is assumed to represent the dynamic of the microbial food web. State variables and partial differential equations are listed in Table 1 and detailed in Appendix A, and parameters definition and values are given in Table 2.

2.3. Coupling With the 3-D Regional Circulation Model

[7] The partial differential equation used to compute the evolution of a simulated scalar (here C) is of the form

$$\frac{\partial C}{\partial t} + u\frac{\partial C}{\partial x} + v\frac{\partial C}{\partial y} + w\frac{\partial C}{\partial z} = \frac{\partial}{\partial x}\left(K_x\frac{\partial C}{\partial x}\right) + \frac{\partial}{\partial y}\left(K_y\frac{\partial C}{\partial y}\right) + \frac{\partial}{\partial z}\left(K_z\frac{\partial C}{\partial z}\right) + \text{sources} - \text{sinks},$$

where t is time, x, y, z are the spatial coordinates, u, v, w are the current velocities in the x, y, z directions, respectively; and K_x, K_y and K_z are the horizontal and vertical eddy diffusion coefficients, respectively; the sinks and sources are described in Table 1. At each time step, the transport of each biological variable is performed by the advection-diffusion routine of the physical model while the sink and source terms are explicitly computed afterwards.

[8] The present simulation covers the 1997 1-year period. This year was chosen because the atmospheric and runoff conditions were close to their respective climatology. The physical and biological models are initialized with observations acquired during November and December 1996 throughout the GSL from the Atlantic Zone Monitoring Program [*Therriault et al.*, 1998]. In order to initialize the biological model with a dynamically balanced physical ocean, the circulation model starts in November 1996 with observed temperature-salinity profiles interpolated to each model layer. It runs until 1 January 1997, at which time the profiles of nitrate and chlorophyll *a* (Chl *a*) from the November-December 1996 observations are in turn interpolated and merged into the simulation. Equal concentrations of large and small phytoplankton were assumed to initiate the run. Because of the lack of data for the remaining biological scalars for the same period, idealized profiles were used. Values of 1 mmol N/m^3 for ammonium [e.g., *Levasseur et al.*, 1990; *Tremblay et al.*, 2000; *Zakardjian et al.*, 2000], 0.05 mmol N/m^3 for DON and 0.005 mmol N/m^3 for PON were assigned to each depth interval from the surface to the last active layer. Concentrations for mesozooplankton and microzooplankton were set to 0.4 mmol N/m^3 [e.g., *Sime-Ngando et al.*, 1995; *Roy et al.*, 2000; *Savenkoff et al.*, 2000] in the upper 25 m and to 0 below this depth. Laterally homogenous initial conditions for the biological scalars were assigned to each grid point. At the open boundaries of the domain, the concentrations are maintained constant through time and are the same as those used for the initial conditions. Both chemical and biological variables are set to zero in the inflowing rivers. A dynamic equilibrium is reached after 2 to 3 weeks in January, mostly affecting the mesozooplankton and nitrate fields (seen in Figures 3a and 3c). Sea ice and winter

Table 1. State Variables and Partial Equations

Symbol	Meaning	Partial Equation
NO3	nitrate	$\frac{dNO3}{dt} = -\mu_{LP}.NuNO3_{LP}.LP - \mu_{SP}.NuNO3_{SP}.SP$
NH4	ammonium	$\frac{dNH4}{dt} = -\mu_{LP}.NuNH4_{LP}.LP - \mu_{SP}.NuNH4_{SP}.SP + ex.MEZ + gz_{MIZ}.(1-eg).(1-ass_{MIZ}).MIZ + rem.DON$
LP	large phytoplankton	$\frac{dLP}{dt} = (\mu_{LP} - m_{LP}).LP - gz_{MEZ}.(\frac{LP}{LP+MIZ}).MEZ - sed_{LP}.\frac{\partial LP}{\partial z}$
SP	small phytoplankton	$\frac{dSP}{dt} = (\mu_{SP} - m_{SP}).SP - gz_{MIZ}.MIZ$
MEZ	mesozooplankton	$\frac{dMEZ}{dt} = gz_{MEZ}.ass_{MEZ}.MEZ - m_{MEZ}.MEZ^2 - ex.MEZ$
MIZ	microzooplankton	$\frac{dMIZ}{dt} = gz_{MIZ}.ass_{MIZ}.MIZ - m_{MIZ}.MIZ - gz_{MEZ}.(\frac{MIZ}{LP+MIZ}).MEZ$
PON	particulate organic nitrogen	$\frac{dPON}{dt} = gz_{MEZ}.(1-ass_{MEZ}).MEZ - m_{LP}.LP - fg.PON - sed_{PON}.\frac{\partial PON}{\partial z}$
DON	dissolved organic nitrogen	$\frac{dDON}{dt} = gz_{MIZ}.eg.(1-ass_{MIZ}).MIZ + m_{MIZ}.MIZ + m_{MIZ}.MIZ - rem.DON$

Table 2. Parameters Used in the Ecosystem Model

Symbol	Meaning	Value and Unit	Reference
	Light Field		
k_w	pure seawater attenuation coefficient	0.04 m^{-1}	*Morel* [1988]
k_p	nonchlorophyllous matter-associated attenuation coefficient	0.04 m^{-1}	fitted
	Phytoplankton		
$k3_{LP}$	LP half-saturation constant for NO3 uptake	1 mmol N/m^3	*Parsons et al.* [1984]
$k4_{LP}$	LP half-saturation constant for NH4 uptake	0.5 mmol N/m^3	
$k3_{SP}$	SP half-saturation constant for NO3 uptake	1 mmol N/m^3	
$k4_{SP}$	SP half-saturation constant for NH4 uptake	0.1 mmol N/m^3	
ke	LP and SP half-saturation constant for light use	10 Ein/m^2/d	*Kiefer and Mitchell* [1983]
dtmin	LP and SP minimum doubling time	0.5 day	*Zakardjian et al.* [2000]
$m_{LP,SP}$	LP and SP senescence	0.02 d^{-1}	fitted
sed_{LP}	LP sinking speed	1 m/d	*Smayda* [1970]
	Zooplankton		
$gmax_{MEZ}$	MEZ maximum grazing rate	0.2 d^{-1}	fitted
$gmax_{MIZ}$	MIZ maximum grazing rate	2 d^{-1}	*Strom et al.* [2001]
iv_{MEZ}	Ivlev parameter of MEZ grazing formulation	0.8 (mmol N/m^3)$^{-1}$	*Frost* [1972]
k_{MIZ}	half-saturation constant for MIZ grazing	0.8 mmol N/m^3	fitted
ass_{MEZ}	MEZ assimilation efficiency	70%	*Kiorbøe et al.* [1985]
ass_{MIZ}	MIZ growth efficiency	30%	*Riegman et al.* [1993]
m_{MEZ}	MEZ mortality	0.05 (mmol N/m^3/d)$^{-1}$	fitted
m_{MIZ}	MIZ senescence	0.02 d^{-1}	fitted
eg	DON egestion by MIZ	30%	*Lehrter et al.* [1999]
ex	NH4 excretion by MEZ	0.05 d^{-1}	*Saíz and Alcaraz* [1992]
	Detritus		
sed_{PON}	PON sinking speed	100 m/d	*Turner* [2002]
fg	PON fragmentation rate	0.05 d^{-1}	*Fasham et al.* [1990]
rem	DON remineralization rate	0.4 d^{-1}	*Packard et al.* [2001]

mixing maintain the biological variables in a slowly varying state until the spring bloom onset.

3. Results

3.1. Mean Seasonal Biomass and Production Cycle

[9] The coupled model produces a strong spatial and temporal variability of planktonic production due to the sea ice dynamics, freshwater runoff, tidal and wind-induced circulation, and mixing. In order to facilitate the interpretation of the model results, we examine the domain-averaged time series over the simulation period (Figure 3). After a relatively low production winter period due to low light intensity and the sea ice cover (January to March), the diatom-dominated vernal bloom occurs in the second half of April following sea ice melt (Figure 3a), increasing light levels and stratification. The simulated timing of the bloom is consistent with previous observations, occurring generally from the end of March to the end of April [*de Lafontaine et al.*, 1991]. The mean depth-integrated (0–45 m) phytoplankton concentration during the peak of the spring bloom, 151 mg Chl *a*/m^2 (Figure 3a), is of the same order of magnitude as observations, with maximum values ranging from 130 mg Chl *a*/m^2 [*Savenkoff et al.*, 2000] to 215 mgChl *a*/m^2 [*de Lafontaine et al.*, 1991]. The coincident peak of primary production is mainly nitrate-based (f-ratio of 0.72, Figure 3b) and reaches 1 g C/m^2/d, a spatially averaged value that is near the lower bound of reported estimates of 1.6–5.7 g C/m^2/d in April [*Tremblay et al.*, 2000]. It reflects the time-differential onset of the spring bloom because maximum values of primary production ranging between 1.4 and 2.2 g C/m^2/d are found over 65% of the GSL in April.

[10] During the development phase of the bloom, the relative contributions of mesozooplankton grazing pressure on large phytoplankton biomass in the euphotic zone, senescence, and sinking of viable cells out of the euphotic zone were similar. At the peak of the bloom, the grazing impact raised to 44%, while senescence and cell sedimentation represented 28.6% and 27.5%, respectively. The decline of the vernal bloom was coincident with the nitrate depletion in the euphotic zone and an increasing grazing pressure from mesozooplankton. Approximately 11 days after the maximum phytoplankton biomass is reached, the model generates a peak of mesozooplankton biomass with a maximum of 2.3 g C/m^2 (Figure 3a), a reasonable value considering that reported mesozooplankton biomass is generally less than 5 g C/m^2 in the GSL [*Roy et al.*, 2000]. This peak of mesozooplankton biomass in May leads to a higher grazing on microzooplankton and then a relaxation of the predation on small phytoplankton, as illustrated by a slight increase of its biomass (Figure 3a).

[11] Following the bloom and the nutrient depletion in the upper layer (Figure 3d), a deep maximum of the phytoplankton biomass develops in the vicinity of the nitracline near 35 m (Figure 3c), as classically observed during the stratified season in the GSL [e.g., *Vandevelde et al.*, 1987; *Levasseur et al.*, 1992; *Ohman and Runge*, 1994; *Runge and de Lafontaine*, 1996] and in other shelf seas [e.g., *Holligan et al.*, 1984]. The simulated deep maximum of phytoplankton biomass is mainly formed by large phytoplankton, whereas small phytoplankton is confined to the upper layer

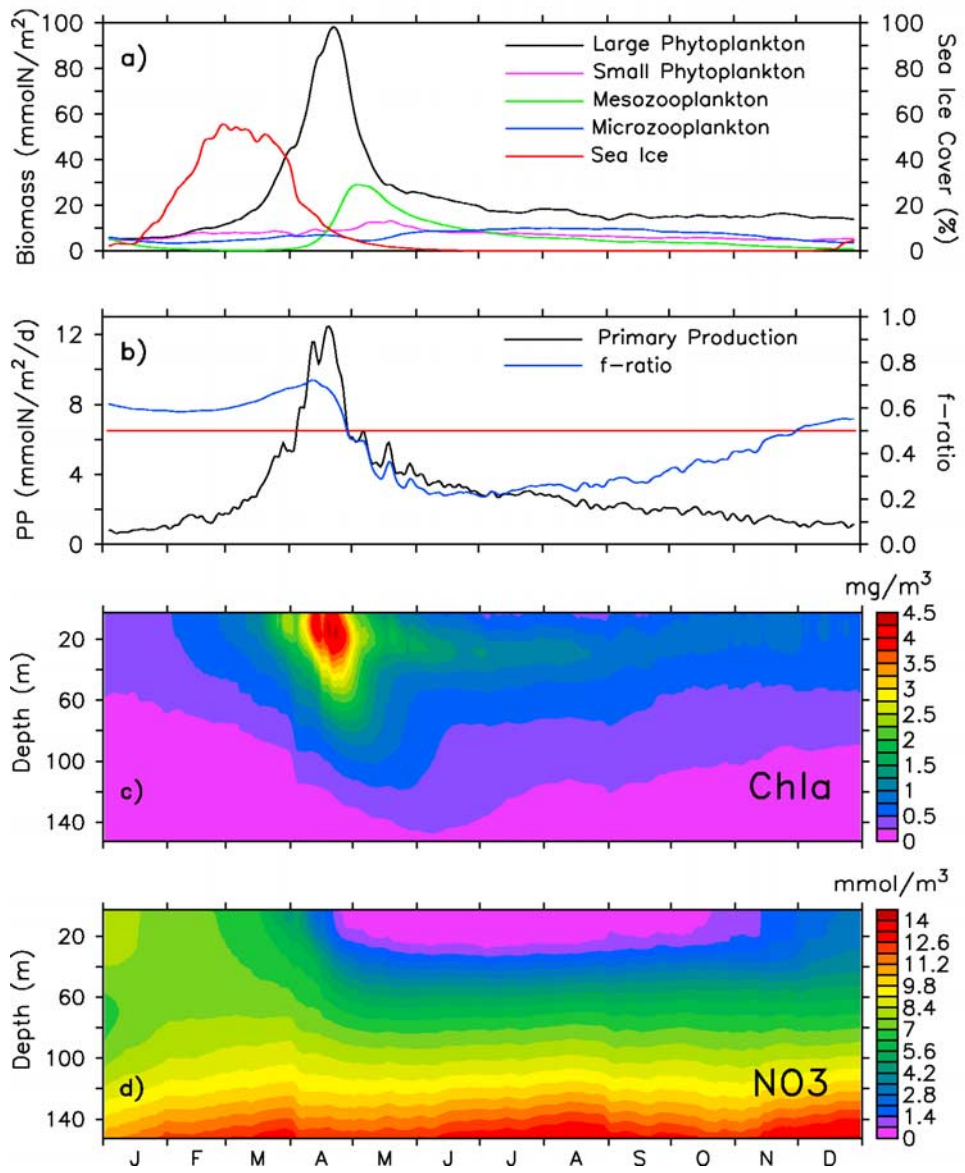

Figure 3. Domain-averaged annual cycle of (a) depth-integrated (0–45 m) biomass of plankton components with sea ice cover, (b) depth-integrated (0–45 m) total primary production with depth-averaged (0–45 m) f-ratio (defined here as the ratio of the total new primary production over total primary production), (c) total chlorophyll *a*, and (d) nitrate. The horizontal line in Figure 3b indicates a f-ratio of 0.5.

(Figure 4). During summer and fall, the large phytoplankton and mesozooplankton biomass gradually decreases to values near those simulated in the preceding winter (February). In contrast, the small phytoplankton and microzooplankton biomass shows only slight variations throughout the year, which is typical in the GSL [*Savenkoff et al.*, 2000]. During summer and fall, the mean domain-averaged biomass of 542 mg C/m^2 for small phytoplankton is comparable to the mean value previously reported for the GSL (636 mg C/m^2 [*Savenkoff et al.*, 2000]). In the same way, the yearly averaged biomass of microzooplankton (0.5 g C/m^2) compares well with seasonal means previously reported for the LSLE (0.55 g C/m^2 in summer [*Sime-Ngando et al.*, 1995]) and the GSL (0.53 g C/m^2 and 0.48 g C/m^2 in winter/spring and summer/fall, respectively [*Savenkoff et al.*, 2000]).

[12] Concomitantly with the phytoplankton biomass, the primary production gradually decreases during summer and fall (Figure 3b). The mean summer primary production is 197 mg C/m^2/d, corresponding to the lower bound previously reported in the GSL (180–504 mg C/m^2/d [*Tremblay et al.*, 2000]). However, the primary production can locally reach values as high as 2.3 g C/m^2/d and 2.6 g C/m^2/d in the GSL and Lower St. Lawrence Estuary (LSLE), respectively. On average, regenerated production prevails in summer (0.21 < f-ratio < 0.30) while the fraction of new production continuously increases in fall (0.30 < f-ratio < 0.55) due to the nitrate replenishment of the euphotic zone from depth (Figure 3b) associated to fall and winter wind-driven mixing. These results compare well with the relative contribution of nitrate to primary production calculated by *Tremblay et al.* [2000] for spring (73%), summer (27%), and fall (10–41%).

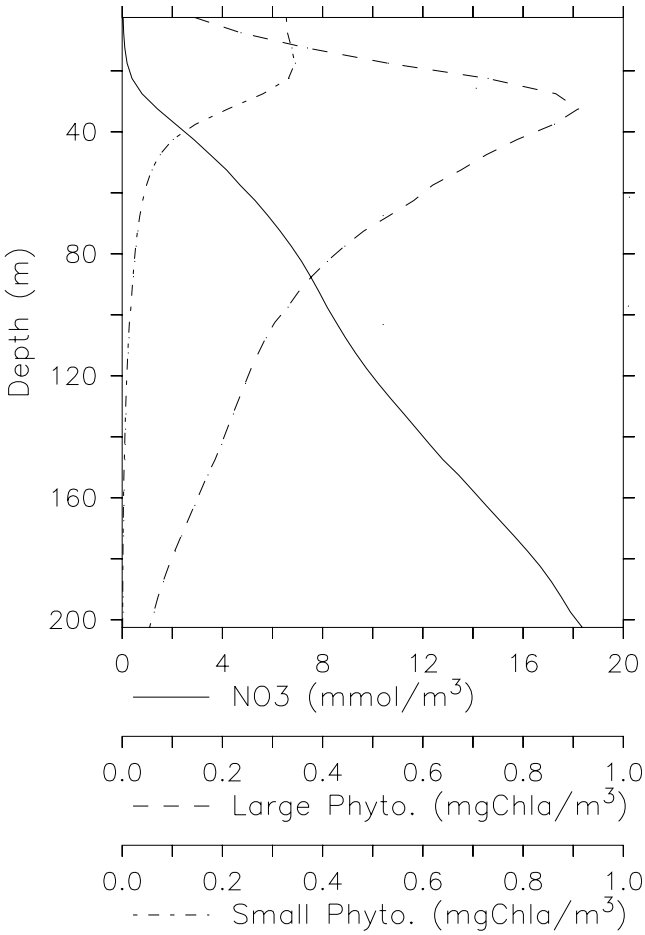

Figure 4. Vertical distribution of the domain-averaged concentrations of nitrate (solid line), large phytoplankton (dashed line), and small phytoplankton (dash-dotted line) on 15 July.

[13] The simulated Chl *a* and nitrate concentrations have been compared with in situ measurements from DFO monitoring cruises made in June and November 1997. Simulated data have been sampled in the model for the same dates and geographical positions (Figure 5a) and interpolated to the bottles' depth levels. The scatterplots compare measured versus simulated values and show the ability of the model to produce the correct order of magnitude of nitrate and Chl *a* concentrations for the two time periods (Figures 5b and 5c). Regarding Chl *a*, the differences between simulated and observed values are mainly within the range of uncertainty owing to the use of fixed C/N and C/Chl *a* known to be highly variable in response to light conditions and nutrient availability. The simulated Chl *a* profiles are within or close to the range of variation of the observed vertical profiles and follow the observed seasonal evolution of the vertical distribution of Chl *a* (Figures 5e and 5g), despite a tendency to overestimate Chl *a* below the euphotic zone in both time periods. This tendency is mainly due to relatively low transfer rate from sinking LP to PON through natural mortality at depth in the model. Simulated and observed nitrate fields are in good agreement near the surface and at depth (Figure 5df) with a tendency for lower simulated nitrate concentration at mid-depth (50–200 m) at the end of the simulation (November). Two hypotheses could account for this tendency. The first one involves the oversimplification of nutrient recycling at depth in the model. Respiratory activity in the intermediate and deep layers is not considered, while it has been recognized as a key process in nutrient dynamics in the GSL [*Savenkoff et al.*, 2001]. A second hypothesis concerns inflowing Labrador Shelf cold waters that spread at mid-depth (50–120 m) along the north coast and leak in the northwestern GSL (NWG) and LSLE in less than a year [*Saucier et al.*, 2003]. The intermediate nitrate gradient would then be sensitive to the nitrate concentrations imposed at the Strait of Belle-Isle which are assumed time invariant in this first version. The

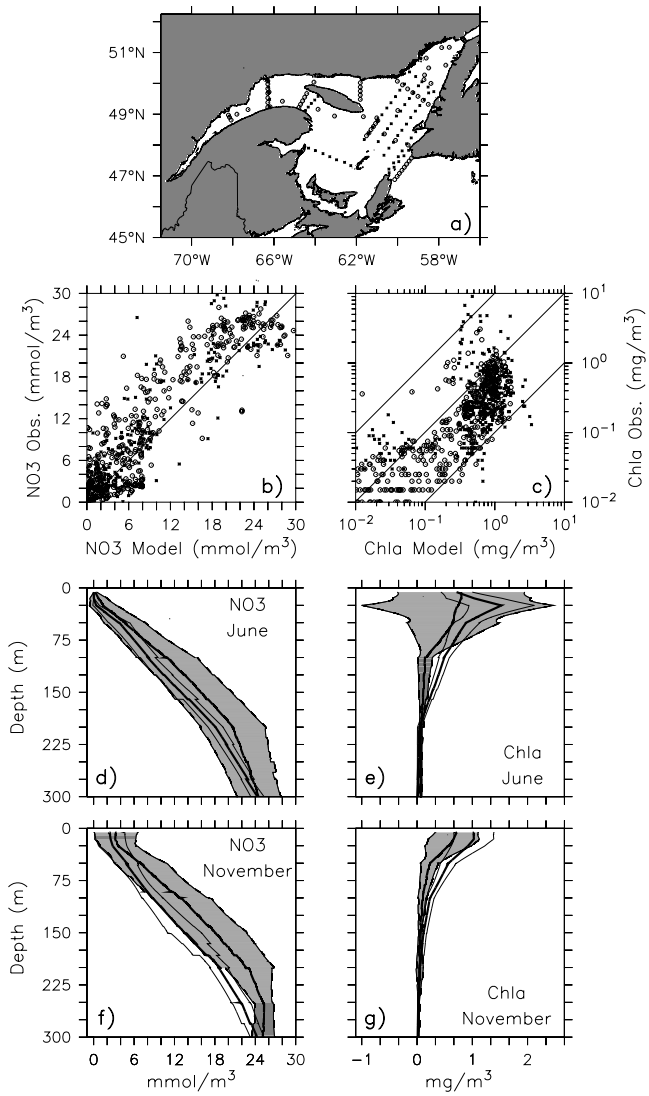

Figure 5. Comparisons of simulated and observed data: (a) sampling locations in June (circles) and November (crosses) 1997, scatterplot of (b) nitrate and (c) total chlorophyll *a*, profiles of simulated (solid line) and observed (dashed line) concentrations of (d) nitrate and (e) total chlorophyll *a* in June and of (f) nitrate and (g) total chlorophyll *a* in November. The thick line represents the spatially averaged profile. The shaded area is delimited by the spatially averaged profile ± standard deviation (thin lines).

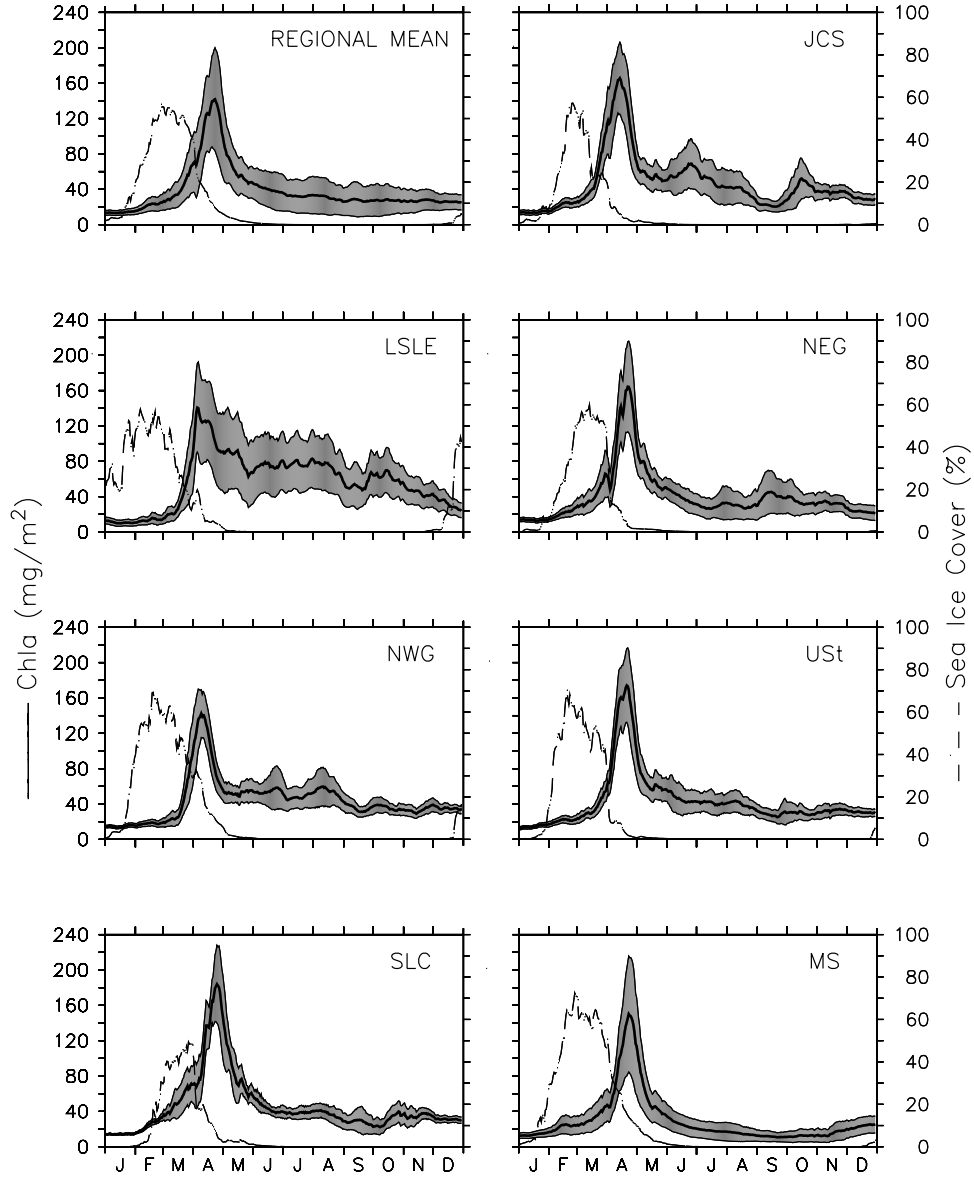

Figure 6. Mean seasonal cycle of total chlorophyll *a* (integrated between 0 and 45 m) and sea ice cover for the numerical domain and all subregions shown in Figure 1. The shaded area is delimited by the spatially averaged time series of total chlorophyll *a* (thick line) ± standard deviation (thin lines).

inflow of Labrador Shelf cold waters is more marked in fall [*Petrie et al.*, 1988; *Saucier et al.*, 2003] and nitrate boundary conditions may also play an important role in the preconditioning of the next year s bloom. Conditions at the Strait of Belle-Isle are generally not well monitored, and limit the precision of both physical and biological models. In spite of that, and considering the overall agreement between simulated and observed nitrate concentrations in the upper 50 m, we are confident that the model reasonably captures the seasonal cycle of primary production in the GSL.

3.2. Subregional Differences in Planktonic Production

[14] Superimposed on the mean annual cycle, the model shows marked differences in the seasonal phytoplankton dynamics among and throughout the subregions of the GSL, as depicted by the mean algal biomass and associated standard deviations. The timing of the phytoplankton spring bloom does not appear to be synchronous with maximum values of phytoplankton biomass occurring from the beginning to the end of April (Figure 6). This spatial variability of the spring bloom timing is mainly due to subregional differences in sea ice distribution, the later sea ice melt being associated with the later blooms, as on the Magdalen Shallow (MS) and northeastern Gulf of St. Lawrence (NEG), a result that is consistent with observations [e.g., *de Lafontaine et al.*, 1991; *Koutitonsky and Budgen*, 1991]. Note that limited sea ice cover in winter (<60%) permits substantial increase of phytoplankton biomass in late February-early March, as in the southern Laurentian Channel (SLC) and NEG (Figure 6), suggesting that light conditions are not limiting during this period. This result is consistent with the substantial levels of phytoplankton biomass

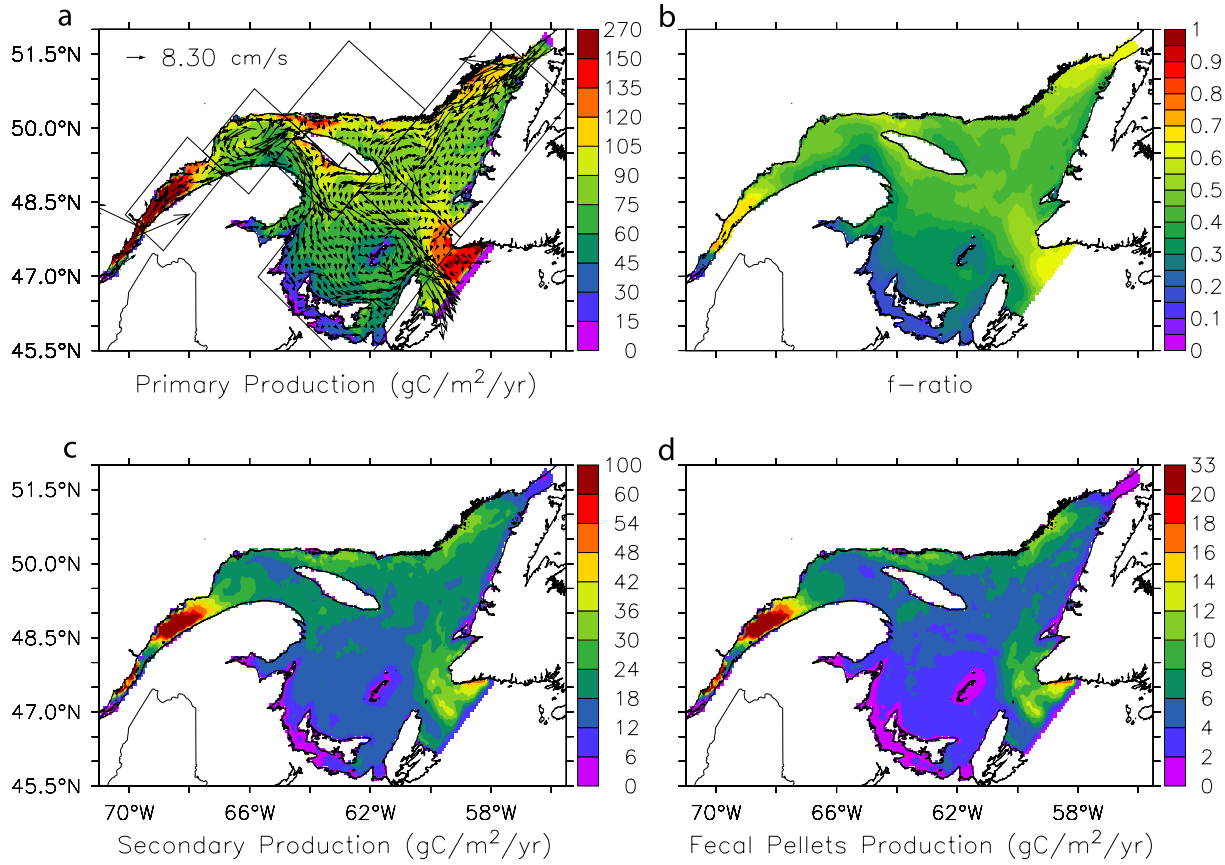

Figure 7. Regional overview of the (a) yearly and depth-integrated (0–45 m) total primary production with yearly and depth-averaged (0–45 m) currents, (b) yearly- and depth-averaged (0–45 m) f-ratio, (c) yearly and depth-integrated (0–45 m) total secondary production, and (d) yearly and depth-integrated (0–45 m) fecal pellets production.

reported in the GSL in late fall–early winter (CJGOFS cruises [e.g., *Roy et al.*, 2000; *Tremblay et al.*, 2000]) and late winter [*Hargrave et al.*, 1985] as well as with the bloom timing in conterminous shelf seas (Narragansett Bay [*Hitchcock and Smayda*, 1977]).

[15] The LSLE, NWG, Jacques Cartier Strait (JCS), and Unguedo Strait (USt) subregions show marked deviations from the mean seasonal cycle, mainly through a higher summer primary production, as illustrated in Figure 6 with the phytoplankton biomass. On an annual basis, these subregions are more productive than the MS, SLC and NEG (Figure 7). The yearly simulated primary production averaged over both the LSLE and GSL is 84 g C/m^2/yr, with local values ranging from less than 50 g C/m^2/yr in the Northumberland Strait to more than 150 g C/m^2/yr in the LSLE and JCS. The primary production in the MS is generally below the mean value (<75 g C/m^2/yr) while that of the NWG, USt, and north coast is above the mean with local values greater than 120 g C/m^2/yr. The high planktonic production in northeastern Cabot Strait is rather due to the continuous input of nitrate related to open boundary conditions. The inflow of Atlantic waters in this area continuously brings nutrient-rich surface waters in the model and generates an artificial area of high planktonic production. Nevertheless, this effect has a limited spatial extent and does not affect the results farther into the GSL. The inflow of Atlantic waters is greater at depth but in a depth range (100–300 m) for which thermohaline and biogeochemical properties are poorly or even unaffected by the seasonal variability (by contrast with sea surface properties).

[16] Highest values of total primary production and f-ratio (Figure 7) are found in subregions where the euphotic zone encounters higher nitrate concentrations. It indicates that increased summer primary production is first controlled by upward transport and turbulent diffusion of nitrate driven by the physical model. Similarly, the lowest nitrate concentrations and primary production rates are produced in the very shallow areas like in the Northumberland Strait and around the Magdalen Islands. Since these areas are not nitrate repleted after its exhaustion during the spring bloom, regenerated production prevails most of the year, as illustrated by the very low annual f-ratio values (about 0.2–0.3). Such spatial variations of primary production are mirrored on the annual secondary and fecal pellets production (Figure 7), showing that increased primary production drives the herbivorous food web first in the model.

[17] The more productive subregion is the LSLE, known to be strongly influenced by tidal upwellings of cold nutrient-rich intermediate waters occurring at the head of the Laurentian Channel [*Steven*, 1974; *Greisman and Ingram*, 1977; *Gratton et al.*, 1988; *Saucier and Chassé*,

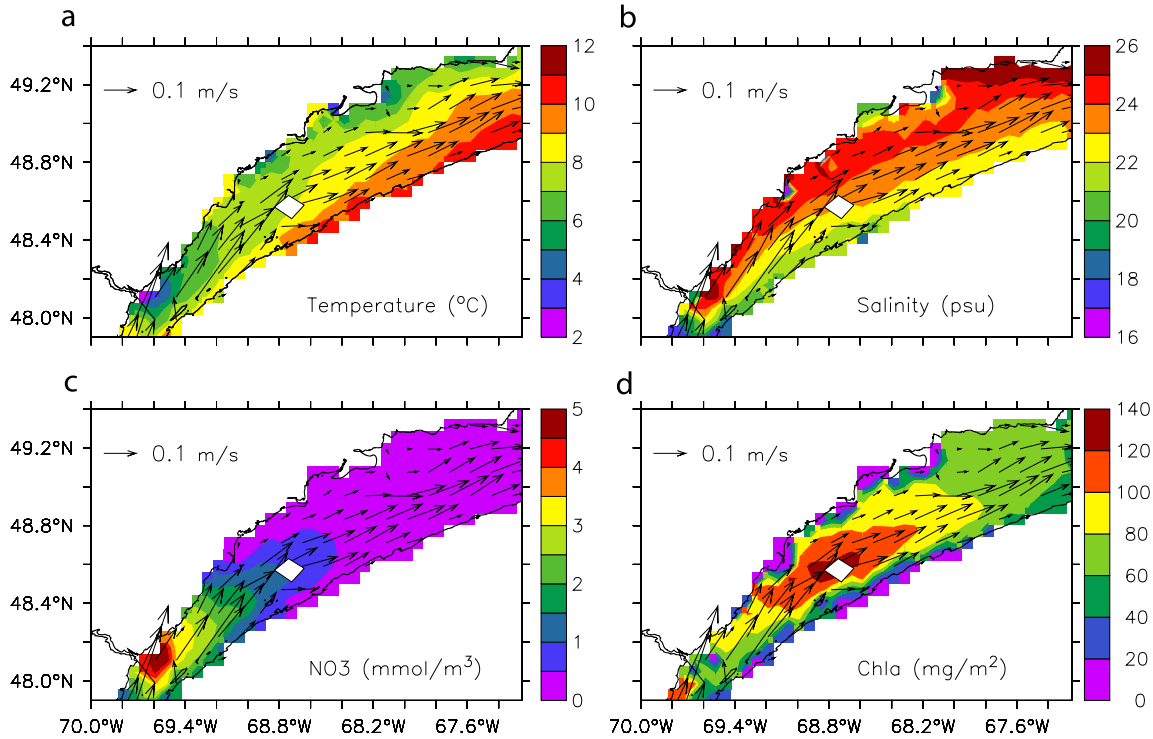

Figure 8. May to October mean in the LSLE of (a) sea temperature (5 m), (b) salinity (5 m), (c) nitrate (5 m), and (d) depth-integrated (0–45 m) total chlorophyll *a*. Mean summer currents (5 m) are overlaid in all panels.

2000]. This so-called "nutrient pump" supports high phytoplankton biomass throughout summer similar to bloom values [*Levasseur et al.*, 1984; *Therriault and Levasseur*, 1985; *Plourde et al.*, 2001], a result well reproduced in the model (Figure 8). The resulting cold sea surface anomaly at the head of the deep through along with higher nitrate concentrations (Figure 8) are clearly evidenced even on a summer mean in the model. Figures 9b and 9c illustrate the effect of the neap-to-spring tidal cycle on the nutrient replenishment of the upper layer through the shoaling of the nitracline and isopycnals. Surface outcrop of low temperature and nutrient-rich waters from the cold intermediate layer is more important during fortnightly spring tides, and results in cyclic increases of phytoplankton biomass [*Sinclair*, 1978; *Demers et al.*, 1986]. In summer, the LSLE assumes one quarter of the total (i.e., the entire numerical domain) vertical advective and diffusive fluxes of nitrate at the bottom of the euphotic zone. These periodic inputs of nitrate considerably enhance primary production that reaches levels close to bloom values throughout the summer (Figure 9a). Figure 8 also illustrates the mean circulation over the summer in the LSLE with the preferential outflow of freshwater on the south coast and the spatial uncoupling between maximum phytoplankton and nitrate concentrations. This spatial uncoupling results from the rapid transport of phytoplankton biomass out of the high nitrate assimilation area (i.e., primary production), as previously described by *Zakardjian et al.* [2000]. However, the model generates a bloom at the beginning of April (Figure 6) in the LSLE, at least 2 months earlier than generally reported [*Sinclair*, 1978; *Levasseur et al.*, 1984; *Therriault and Levasseur*, 1985; *Sime-Ngando et al.*, 1995; *Roy et al.*, 1996; *Plourde et al.*, 2001]. The late bloom in the LSLE is thought to be due to a combination of turbidity-induced light limitation and flushing related to the freshwater runoff [*Therriault and Levasseur*, 1985; *Zakardjian et al.*, 2000].

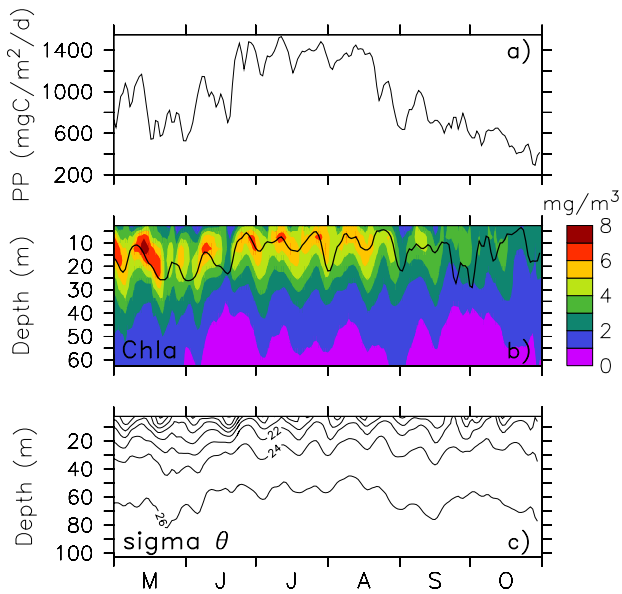

Figure 9. Time course at a fixed station located in the upstream part of the LSLE (white box in Figure 8) of the (a) total primary production (PP), (b) vertical profile of total chlorophyll *a* with the depth of the nitracline overlaid, and (c) vertical profile of density (kg/m^3).

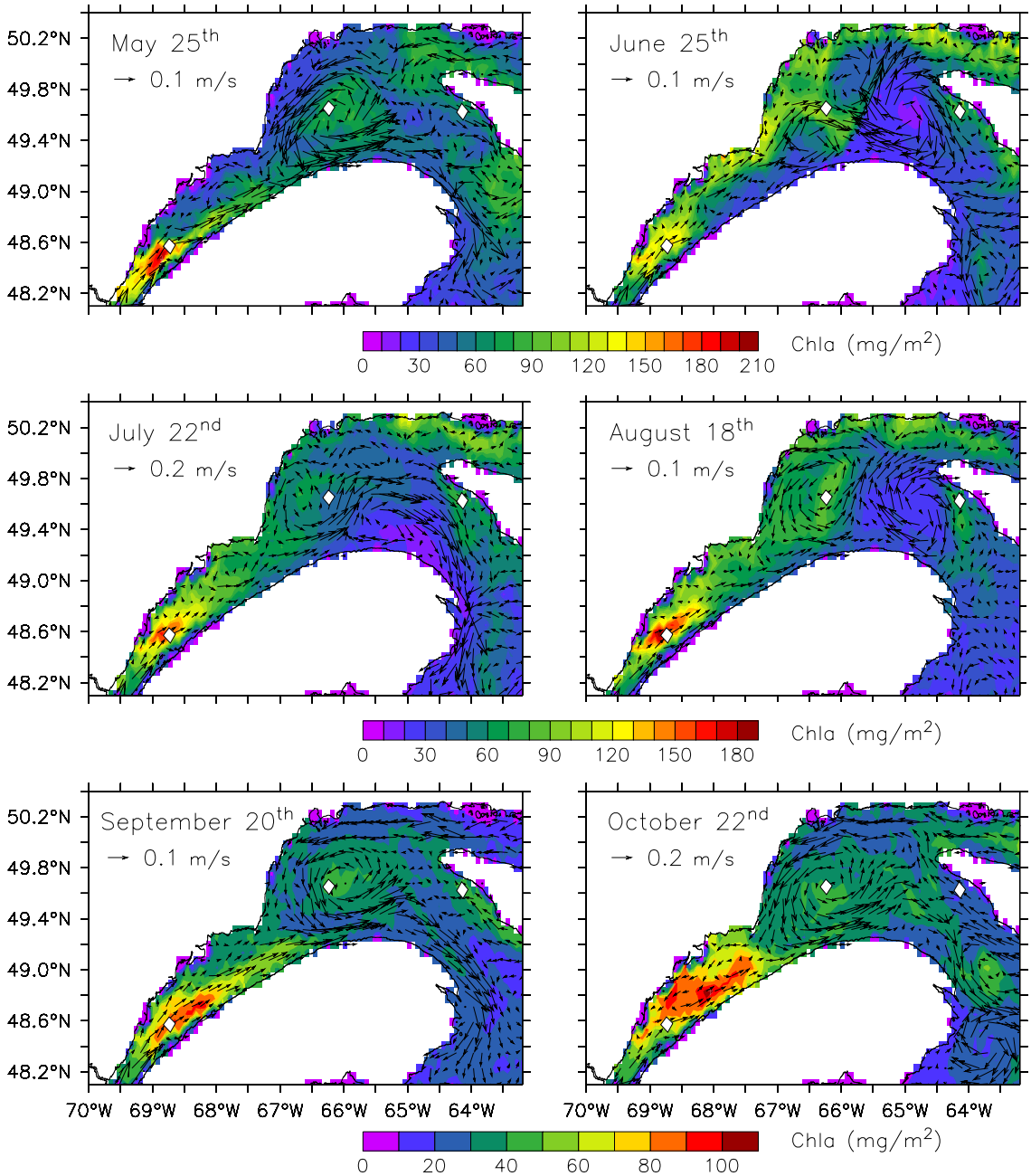

Figure 10. Snapshots of depth-integrated (0–45 m) total chlorophyll *a* (mg/m^2) with depth-averaged (0–45 m) currents on 25 May, 25 June, 22 July, 18 August, 20 September, and 22 October over the LSLE, NWG and the northern USt.

The light field formulation does not include the freshwater-induced turbidity due to nonchlorophyllous material drained by the rivers during the freshet. Consequently, the maximum depth of the simulated euphotic zone in the LSLE is similar to that of the GSL (40 m), i.e., that is twice as deep as generally observed in the estuary (15–20 m [*Therriault and Levasseur*, 1985; *Sime-Ngando et al.*, 1995]). Hence the simulated early bloom in the LSLE is due to unrealistic light conditions in spring.

[18] The NWG is characterized by a marked mesoscale variability that manifests through instabilities of the Gaspe Current and the occurrence of fronts and eddies generated by buoyancy and wind forcing [*Benoit et al.*, 1985; *Mertz et al.*, 1988; *Koutitonsky and Budgen*, 1991; *Sheng*, 2001]. Figure 10 illustrates such a strong mesoscale variability of the circulation (depth-averaged currents from the surface to 45 m) and its impact on phytoplankton biomass (depth-integrated Chl *a* from the surface to 45 m) from spring to fall. In May, the currents show a typical situation characterized by a well-established cyclonic Anticosti Gyre and a Gaspe Current close to the south shore [e.g., *El-Sabh*, 1976], where the phytoplankton biomass is twice higher than in the adjacent waters (80–90 mgChl *a*/m^2 versus 40 mg Chl *a*/m^2). A dipole-like structure is generated in

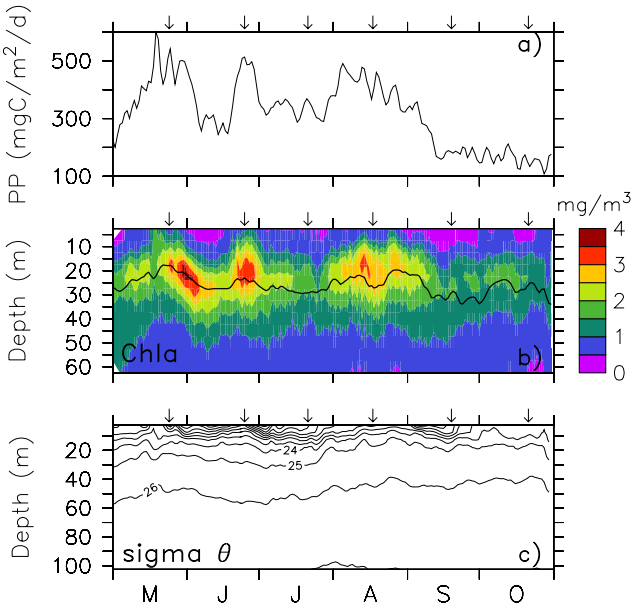

Figure 11. Time course at a fixed station located in the NWG (white box in Figure 10) of the (a) total primary production (PP), (b) vertical profile of total chlorophyll *a* with the depth of the nitracline overlaid, and (c) vertical profile of density (kg/m^3). Vertical arrows indicate each snapshot of Figure 10.

August with a downstream anticyclonic gyre linked to a slow-growing instability of the Gaspe Current starting in late June in the model, a known feature of the NWG circulation [*Mertz et al.*, 1988; *Benoit et al.*, 1985; *Sheng*, 2001]. Later in fall (September and October), the anticyclonic gyre weakens, leading to the prevailing of the cyclonic gyre with consistently higher phytoplankton biomass in its center and in the Gaspe Current. Figure 11 shows the spring to fall local variability of the density stratification, nitracline depth, and vertical distribution of Chl *a* in the center of the Anticosti Gyre. Higher Chl *a* concentrations and primary production rates are associated with the uplifting of the nitracline and isopycnals in response to vertical motions governed by this mesoscale activity that hence controls the phytoplankton development in summer (Figure 11).

[19] The model simulates higher production values mainly mediated by the herbivorous food web (see Figure 7) along the southern Anticosti Island and the north coast, two areas subject to wind-induced upwellings [*Fuentes-Yaco et al.*, 1995, 1996, 1997a, 1997b; *Rose and Leggett*, 1988; *Saucier et al.*, 2003]. In the shallow western JCS, this higher productivity is reinforced by tidal mixing that characterizes this area [e.g., *Koutitonsky and Budgen*, 1991]. The higher productivity of the USt due to wind-induced upwelling activity along the southern Anticosti Island has already been highlighted by annual and seasonal composites and daily CZCS images of pigment concentration [*Fuentes-Yaco et al.*, 1995, 1996, 1997a]. Nevertheless, the USt is also strongly influenced by the Gaspe Current outflow [*Mertz et al.*, 1988], and the interaction of wind-induced upwellings with the Gaspe Current variability leads to a more complex situation than previously qualified in this region [e.g., *Fuentes et al.*, 1996, 1997a] (see Figure 10). Figure 12 illustrates such a simulated upwelling events occurring along the northwestern Anticosti Island on 21 September where a patch of high phytoplankton, mainly dominated by large algae (not shown), develops following a northwesterly wind events. In the following days, the wind-induced phytoplankton patch spreads in the USt owing to transport by the Gaspe Current and circulation along Anticosti Island.

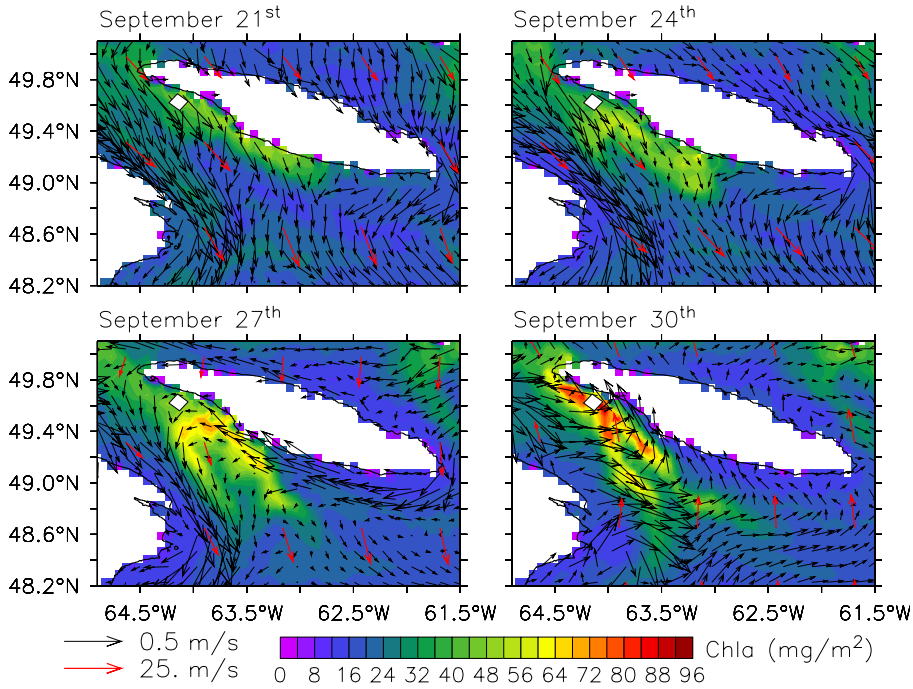

Figure 12. Snapshots of depth-integrated (0–45 m) total chlorophyll *a* with depth-averaged (0–45 m) currents and surface winds on 21 September, 24 September, 27 September, and 30 September in the USt.

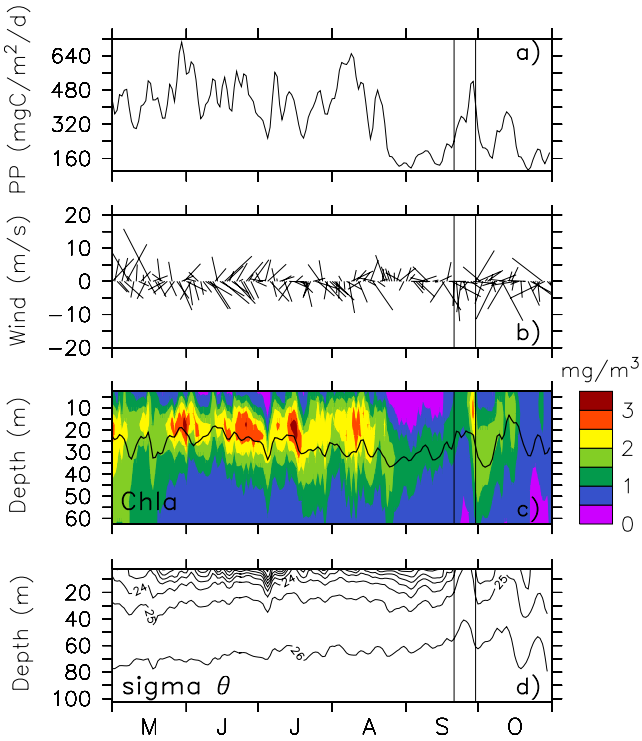

Figure 13. Time course at a fixed station located in the USt (white box in Figure 12) of the (a) total primary production (PP), (b) surface winds, (c) vertical profile of total chlorophyll *a* with the depth of the nitracline overlaid, and (d) vertical profile of density (kg/m^3). The two vertical solid lines delimit the time period of the upwelling events shown in Figure 12.

The strong current shear induced by this complex circulation locally uplifts the nitracline and isopycnals, leading to an increase of the phytoplankton biomass and production (Figures 12 and 13). Such an offshore transport of phytoplankton pigments, from the west coast of the Anticosti Island toward the MS, was reported by *Fuentes-Yaco et al.* [1995, 1996]. Figure 13 shows that these episodic inputs of nitrate in the euphotic zone frequently occur throughout the summer at the synoptic scale similar to that of wind events.

[20] In addition to the relatively well-known features described above, the model reveals patterns of higher planktonic production associated with Labrador Shelf waters entering the GSL through the Strait of Belle-Isle in late summer and fall. Labrador Shelf water inflows, with mean simulated transport rates between 0.2 Sv (summer and spring) and 0.4 Sv (fall and winter [see also *Petrie et al.*, 1988]), are pulsed-like and spread along the north coast of the GSL. Such an event, occurring in late September–early October, is illustrated in Figure 14 by a westward migrating sea surface temperature anomaly and an associated phytoplankton patch. The Chl *a* patterns closely follow the isolines of temperature as the cold surface waters spread westward. Figure 14 also presents a 4-day (27–30 September) SeaWiFS composite image that reveals a very similar patch of Chl *a*. The surface Chl *a* concentrations produced by the model are within 2–3 mg/m^3 of the SeaWiFS-derived values and, while the observed and simulated patches are not strictly coincident in time, they have similar spatial structures. Depth-integrated (0–45 m) phytoplankton biomass in the patch reaches bloom-like values (>100 mg Chl *a*/m^2) contrasting with the lower levels in the surrounding waters (20–40 mg Chl *a*/m^2). The significant increase in algal biomass appearing on the mean seasonal cycle of the NEG and JCS (Figure 6) in September and October, respectively, is due to this feature. The occurrence of such episodic events in summer and fall (see Figure 15) is linked to Labrador Shelf water inflows, as shown by the moving window-averaged (14 days) time series on which high-frequency perturbations and spring-neap tides are removed (Figure 15e). A pulse of water is associated with a time lag of 3–4 weeks to a surface outcrop of Labrador water through the euphotic zone due to wind-driven mixing, complex topography in this area, and local hydrodynamic processes related to the spreading of the pulse (7–10 cm/s). The uplifted waters are colder, saltier, and nutrient rich and substantially enhance algal biomass and primary production (Figures 15a–15d).

[21] In the MS, SLC, and NEG, the summer phytoplankton biomass is low in comparison to the subregions described above. The low production on the MS is related to the rapid nutrient depletion in spring, the strong thermocline and higher surface stratification in summer that limit the nitrate replenishment of the euphotic zone from depth [e.g., *Hargrave et al.*, 1985]. In summer, inputs of allochthonous nutrients on the MS can only originate from advective transport from the SLC and NWG through the two branches of the mean freshwater seaward circulation (Figure 7a). Figure 16 illustrates the mean summer nitrate concentration and horizontal currents along a SW-NE transect across the MS and the Laurentian Channel. When leaving the USt, the Gaspe Current outflow (Figure 16a) forms two main branches of freshwater seaward circulation, one inshore and the other at the shallow edge of the MS (Figures 16b and 16c), characterized by velocities ranging from 8 cm/s to 18 cm/s, respectively. The model shows that the nutrient transport through the seaward circulation does not significantly affect the southern MS primary production given the low nitrate concentration in the transported waters.

[22] While the peak of primary production is similar to that of the more productive subregions, and even higher in the SLC, annual planktonic production in the NEG and SLC is low owing to low summer production (Figure 7). The spring bloom intensity is mainly dependent on nitrate replenishment from depth associated with winter mixing. This process may be higher in the SLC (Figure 6) where deep mixing occurs owing to sea ice formation and winds. Wind-driven mixing is the main process allowing nutrient replenishment of the euphotic zone in summer in these subregions where relatively low mesoscale activity prevails. The persistent pigment minimum reported along the west coast of Newfoundland [*Fuentes-Yaco et al.*, 1997a], where southerlies would drive a downwelling circulation [*Gilbert and Pettigrew*, 1993], is well reproduced by the model (see Figure 7).

4. Discussion

[23] The present model was developed to gain a better understanding of the effect of the climatic and oceanographic conditions on planktonic production in the Gulf

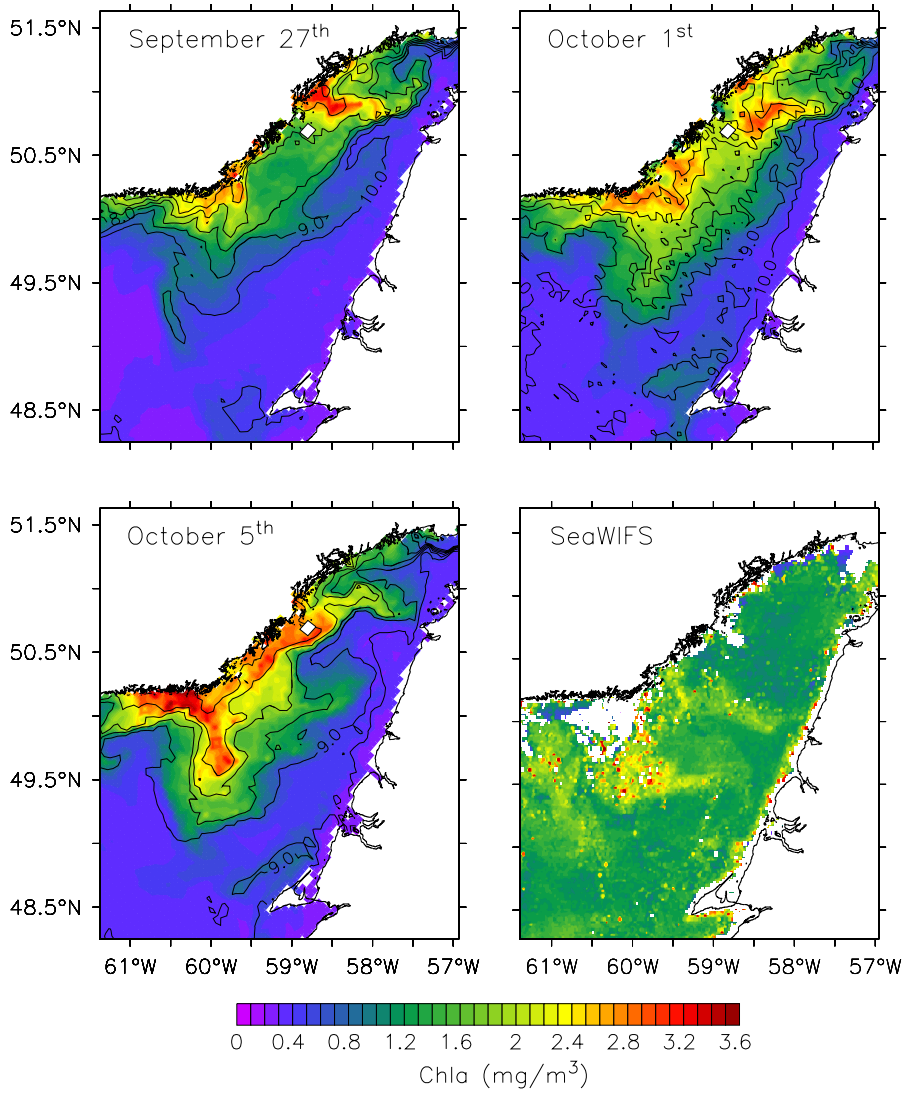

Figure 14. Snapshots of total chlorophyll *a* (5 m) with sea temperature contours (5 m, °C) on 27 September, 1 October, and 5 October. A 4-day (27–30 September) SeaWiFS composite image is presented in the bottom right panel.

of St. Lawrence. Given the richness of the physical processes in this coastal oceanographic system, described by *Koutitonsky and Budgen* [1991] and simulated by *Saucier et al.* [2003], we chose to use a moderately complex planktonic ecosystem model to approximate the biological response to the high frequency to seasonal variations of environmental conditions generated by the sea ice-ocean model. While the planktonic ecosystem model is more simple than the biogeochemical model of *Tian et al.* [2000, 2001], solutions produced by the coupled model at the regional and subregional scale are overall in agreement with historical data. It produces a mean (i.e., spatially averaged over the numerical domain) seasonal cycle dominated by a large phytoplankton spring bloom followed by the development of a deep maximum of phytoplankton biomass persistent in summer and the prevailing of regenerated production, as classically described in the region [e.g., *de Lafontaine et al.*, 1991; *Savenkoff et al.*, 2000; *Tremblay et al.*, 2000; *Tian et al.*, 2000, 2001].

[24] The model does not generate any significant fall bloom at the regional scale but reveals fall blooms related to local environmental conditions such as pulsed inflows of Labrador Shelf water along the north coast (Figure 6). The fall bloom is a well-known feature of the primary production cycle in temperate coastal seas. It is induced by increased wind-driven turbulent mixing during autumn storms that erode the summer stratification, favoring the nutrient replenishment of the impoverished surface layer and hence phytoplankton growth until light availability becomes limiting in early winter. The absence of a regional fall bloom in the simulation may come from the low wind regime in fall 1997: While the wind-forcing database used to drive the physical model presents strong wind events in fall 1997 (up to 20 m/s), those do not generate any significant mixing events at the regional scale. This result is supported by biweekly composite SeaWiFS images for 1997. Preliminary runs made for 1998 and 1999 with the same model configuration generate marked fall bloom

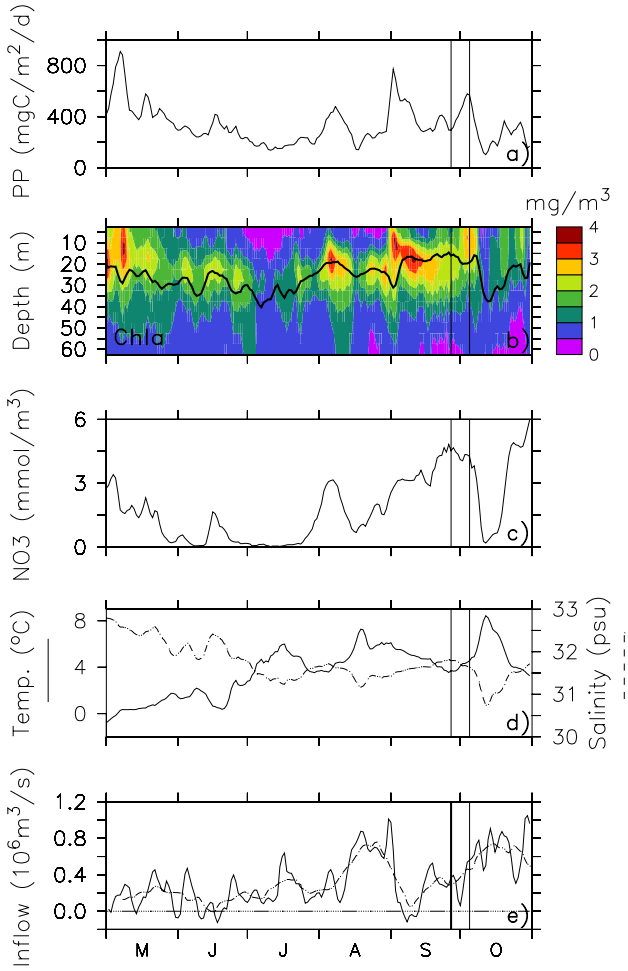

Figure 15. Time course at a fixed station located in the NEG (white box in Figure 14) of the (a) total primary production (PP), (b) vertical profile of total chlorophyll *a* with the depth of the nitracline overlaid, (c) nitrate concentration at 25 m, (d) temperature and salinity at 25 m, and (e) net water transport across the Strait of Belle-Isle with its moving window-averaged (14 days) equivalent overlaid. The two vertical solid lines delimit the time period of the simulated events shown in Figure 14.

underlining the strong interannual variability of the GSL physical conditions in fall.

[25] Superimposed on the mean annual cycle, the model generates a marked heterogeneity of summer planktonic production in the Lower Estuary and the Gulf of St. Lawrence. Different physical processes (tidal mixing, buoyancy-driven circulation, wind-induced coastal upwelling) drive the nutrient availability for phytoplankton, and consequently primary production events with different time and space scales. The model reproduces the high summer planktonic production in the LSLE, which is largely due to nutrient fluxes driven by the high tidal mixing in this subregion [*Levasseur et al.*, 1984; *Therriault and Levasseur*, 1985; *Levasseur and Therriault*, 1987]. It also generates coastal upwellings along the north coast of the GSL and the western Anticosti Island which are shown to increase the algal biomass, dominated by large phytoplankton, and planktonic production. Widely distributed year-round, wind-induced coastal upwellings are known to have a marked effect on oceanic heat fluxes [*Saucier et al.*, 2003] and phytoplankton pigments [*Fuentes-Yaco et al.*, 1995, 1996, 1997a, 1997b] in the GSL. The buoyancy-driven circulation induced by the runoff of the St. Lawrence Estuary shows a typical mesoscale variability acting on a weekly to seasonal timescale that leads to a higher productivity in the NWG. The very high phytoplankton biomass regularly observed in the Gaspe Current [*Sévigny et al.*, 1979; *Levasseur et al.*, 1992] was not always clearly reproduced by the model, particularly in spring and fall. *Levasseur et al.* [1992] suggested that the high phytoplankton biomass in the Gaspe Current in spring may result from the advection of high biomass from the estuarine waters (see Figure 10). The fact that the model does not include the higher turbidity of estuarine waters and overestimates the nitrate consumption in the LSLE explains the low nutrient concentration and phytoplankton biomass in the Gaspe Current in spring. Summer observations in the Gaspe Current have revealed nutrient-impoverished and low phytoplankton conditions in the jet while secondary circulation may increase nutrient availability and primary production in the frontal zone between the estuarine and gulf waters [*Levasseur et al.*, 1992]. These observations are more coherent with our simulation, but this frontal-induced higher productivity may be underestimated in the model. The

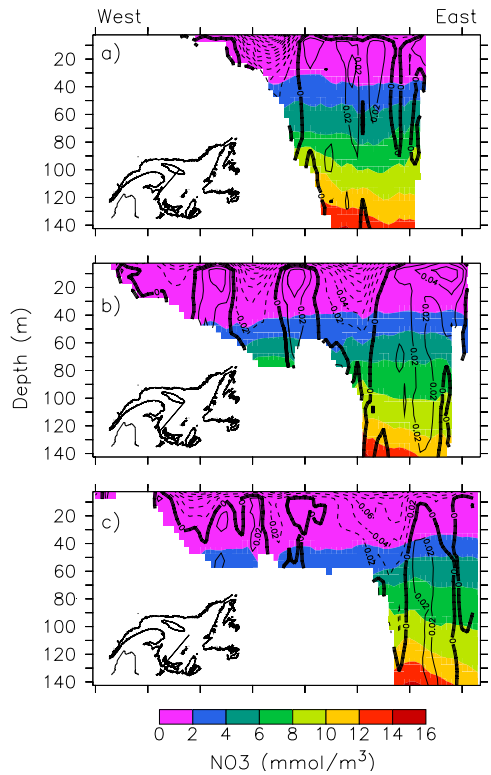

Figure 16. Vertical sections from the MS toward the Laurentian Channel illustrating the nitrate concentration and the NW-SE current (m/s) averaged over July–August. The dashed and solid lines represent the seaward and northwestward current, respectively. On each panel, the transect is indicated on the map.

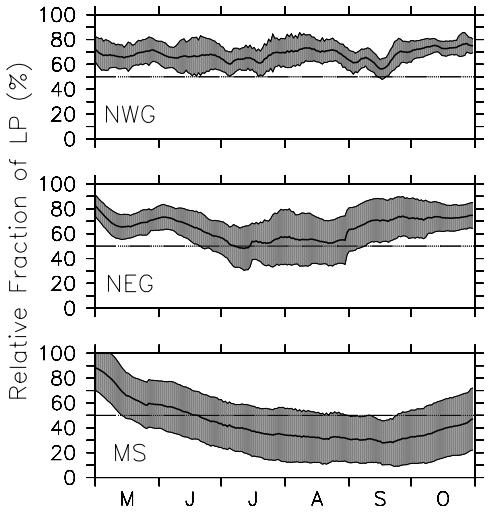

Figure 17. Time course of the depth-averaged (0–45 m) relative concentration of large phytoplankton (LP) averaged over the NWG, the NEG, and the MS (bold line). The shaded area is delimited by the mean ± standard deviation (thin lines).

spatial resolution of the model being half to one third of the baroclinic Rossby radius of deformation in this subregion (10–15 km), the model is able to generate mesoscale features, but frontal-induced increased phytoplanktonic production often results of submesoscale processes [e.g., *Woods*, 1988; *Zakardjian and Prieur*, 1998] which may not be resolved with the present resolution. *Mahadevan and Archer* [2000] and *Lévy et al.* [2001] examined the effect of model resolution on resolving vertical motions, nutrient flux, and primary production in mesoscale and frontal structures and have shown that regional primary production increases with the model resolution. The simulated NWG production and its impact on downstream areas may thus be underestimated. Nevertheless, it is clearly evident that the mesoscale variability associated to the buoyancy-driven circulation in the LSLE, NWG, and USt plays a fundamental role in the dynamics of planktonic production in these subregions of the GSL.

[26] The model also simulates the effect of hydrodynamics on the competition between the herbivorous and microbial food webs, a prerequisite for estimating carbon flux as it is known that the ecosystem structure drives the carbon flux at depth [e.g., *Legendre and Le Fèvre*, 1995; *Longhurst and Harrison*, 1989; *Legendre and Michaud*, 1998; *Legendre and Rivkin*, 2002]. Highest variations of biomass in the mean seasonal cycle concern the herbivorous food web, while the simplified microbial food web constitutes a background of biomass with only slight variations throughout the year, as previously reported in the GSL [*Tremblay et al.*, 1997; *Doyon et al.*, 2000] and on the Scotian Shelf [*Mousseau et al.*, 1996; *Dauchez et al.*, 1996]. Large phytoplankton biomass and production were found to be favored in summer in the frontal zone of the Gaspe Current, which is known to be a highly productive system [*Fortier et al.*, 1992; *Levasseur et al.*, 1992; *Tremblay et al.*, 1997]. In response to tidal mixing, wind-induced coastal upwellings, buoyancy-driven gyres, frontal zones, and eddies, the model generates higher large phytoplankton production and biomass that stimulates the activity of the herbivorous food web (Figure 7) compared to less dynamic subregions. The increased activity of the herbivorous food web in response to mesoscale circulation is a well-known feature in oceanic environments [e.g., *Thibault et al.*, 1994; *Peinert and Miquel*, 1994; *Ressler and Jochens*, 2003]. The dominance of small phytoplankton biomass on the bulk of Chl *a* in summer [*Sévigny et al.*, 1979; *Ohman and Runge*, 1994; *Claereboudt et al.*, 1995; *Tamigneaux et al.*, 1997, 1999; *Tremblay et al.*, 1997, 2000] is not evident on the mean seasonal cycle (Figure 3a) but is more obvious at smaller scales: Less productive subregions show a decrease of the large versus total phytoplankton ratio in summer compared to more productive ones, as illustrated in Figure 17. By comparison with the NWG always clearly dominated by diatoms, the higher standard deviation in July and August in the NEG indicates that small phytoplankton can locally constitute 60–70% of the bulk of the algal biomass. In less productive subregions, such as the MS, the small phytoplankton dominates the bulk of Chl *a* throughout summer. These results highlight the variability that prevails at different scales in the GSL and shows that the model produces the correct trend.

[27] The mean annual primary production computed for the whole Estuary and Gulf (84 g C/m^2/yr), resulting from this high-resolution physically driven numerical experiment, is low in comparison with previously reported estimates of 212 g C/m^2/yr [*Steven*, 1974] and 288 g C/m^2/yr [*Roy et al.*, 2000]. The overall agreement between observed and simulated nitrate concentrations tends to support the order of magnitude of our simulated new primary production but, regarding summer primary production, a key process probably oversimplified in the model concerns nitrogen recycling mediated through microbial trophic pathways. It would be particularly important in the shallow southern MS where a rapid turnover of the organic matter in the euphotic zone, rather than nutrients diffusion from depth, is thought to drive most of the summer primary production [*Hargrave et al.*, 1985]. A microbial activity is implicitly included in the planktonic ecosystem model by way of constant transfer rates governing the breakdown of PON into DON and subsequent DON ammonification. This parameterization assumes a constant bacterial activity throughout the year, while it has been reported to double from the winter-spring to the summer-fall period in the GSL [*Savenkoff et al.*, 2000]. In addition, there is some evidence about the temperature control of bacterial activity in cold coastal waters [*Pomeroy and Deibel*, 1986]. The inclusion in the model of a bacterial component with temperature-dependent biological rates would delay the DON ammonification with a subsequent increase of regenerated production later in summer [e.g., *Tian et al.*, 2001] but is not expected to produce a twofold increase of annual primary production. PON residence time in the euphotic zone is also a critical parameter in regard to regenerated primary production shown to increase as the sinking rate decreases [*Ducklow and Fasham*, 1992; *Crise et al.*, 1999]. In the model, the PON flux at the bottom of the euphotic zone summed over the April-May period is equivalent to 11.6 g C/m^2 (using a C/N ratio of 6.625) and its regener-

ation in the euphotic zone would represent an increase of 14% of our annual estimate of primary production.

[28] Primary production is tightly linked to zooplankton dynamics through nutrient recycling and top-down control, and the lack of pertinent zooplankton data, which are much more time expensive to acquire than primary production related variables, is often a weakness of NPZD modeling [e.g., *Franks*, 2002; *Runge et al.*, 2005]. While we do not have sufficient data to validate zooplankton results, it is important to discuss here the robustness of the model in view of the general knowledge on grazers' dynamics in the GSL and more generally in temperate and high-latitude coastal seas. The simulated annual secondary production of mesozooplankton averaged over the domain reaches 12.6 g C/m^2 and 16 g C/m^2 when integrated over the euphotic zone and all the water column, respectively. Such values are within the range given by *Koski et al.* [1999] in the southwestern coast of Finland, i.e., 10.5–28.1 g C/m^2. Concerning microzooplankton, we do not report in the literature any annual production estimate in coastal waters. Nonetheless, *Levinsen and Nielsen* [2002] estimate to 20–60% the annual primary production processed by ciliates in high-latitude coastal environments. In regard to that study, the fraction of small phytoplankton primary production transferred to microzooplankton biomass calculated by the model (26.7%) is consistent, considering that microzooplankton only grazes on small phytoplankton. On an annual basis, 24.2% of the simulated total primary production is channeled toward the total secondary production, an estimate that fits in the range (20–30%) given by *Legendre and Rassoulzadegan* [1999]. It can be assumed that, on an annual basis, the coupled model simulates a grazers' dynamics consistent with general findings on planktonic production in temperate and high-latitude seas.

[29] Note finally that the simulated primary production is calculated from nitrogen uptake using a fixed Redfield-type C/N ratio thus assuming that carbon and nitrogen dynamics are coupled, an assumption still in debate for mid- and high-latitude regions [e.g., *Sambrotto et al.*, 1993; *Daly et al.*, 1999]. Carbon and nitrogen metabolisms can be temporally uncoupled, especially during nitrogen depletion, with dissolved inorganic carbon uptake that can exceed nitrogen uptake [*Dubinsky and Berman-Frank*, 2001; *Engel et al.*, 2002]. Hence the simulated primary production derived from the Redfield-type ratio may represent a lower bound. Using an algal C/N ratio of 8.5 [e.g., *Grégoire and Beckers*, 2004], the simulated primary production reaches 108 g C/m^2/yr (an increase of 28%). When summed to the PON flux (15 g C/m^2/yr with a C/N ratio of 8.5), it gives an estimate that is 46% higher (123 g C/m^2/yr) than the primary production obtained when using a Redfield-type C/N ratio (84 g C/m^2/yr). Nevertheless, this new estimate of the maximum expected annual primary production remains half those estimated by *Steven* [1974] and *Roy et al.* [2000].

[30] The mean annual primary production computed by the model is the first estimate in the GSL that integrates hourly to seasonal fluctuations of both physical and biological processes concomitantly with a high spatial resolution and complete evenly weighted time-space coverage. Given the overall agreement between simulated and observed nitrate and Chl *a* concentrations (Figure 5), the model reasonably captures the natural variability of nitrate and Chl *a* vertical distribution. Moreover, the striking agreement between the simulated and SeaWiFS-derived surface Chl *a* concentrations in late September in the NEG (Figure 14) demonstrates the ability of the model to generate local transient events that can hardly be evidenced with the usual sampling scheme at sea. Lately, local daily primary production rates computed by the model are well within the range of measured values in the Gulf of St. Lawrence. We suggest that the low mean annual primary production given by the coupled model comes from the weight of the less productive subregions (MS and NEG) in the spatial averaging as the locally computed annual primary production rates are close to reported values in highly productive subregions, such as the LSLE (104 g C/m^2/yr [*Levasseur and Therriault*, 1985]). The *Steven* [1974] estimate of the gulf mean annual primary production was derived from an extensive data set covering the GSL and the main production period (May–September) by extrapolating hourly production rates (among the highest reported for the GSL) on the basis of monthly mean lightly period and, consequently, tends to be overestimated (M. Gosselin, personal communication, 2004). Annual primary production estimated by *Steven* [1974] for the LSLE (508 g C/m^2/yr) is fivefold higher than the value given by *Therriault and Levasseur* [1985] (104 g C/m^2/yr) which is closer to the model solution (154 g C/m^2/yr). The CJGOFS estimate of 288 g C/m^2/yr from *Roy et al.* [2000] results from a limited set of observations (five stations visited 2–6 times between 1992 and 1994) that is far from the spatiotemporal resolution of the model. The annual estimate was made by extrapolation of two seasonal means of daily primary production (winter-spring and summer-fall [*Savenkoff et al.*, 2000]). The winter-spring mean (1358 mg C/m^2/d [*Savenkoff et al.*, 2000]) takes into account the spring bloom and relatively high but punctual winter values. Extrapolated over the winter-spring period (157 days), it results in an estimate (213 mg C/m^2/yr) similar to the Steven annual primary production (212 g C/m^2/yr) that largely overestimates the winter production. Time resolution being a key parameter in estimating primary production [*Wiggert et al.*, 1994], it is clear that extrapolation of sparse measurements over an annual estimate would be imprecise in a highly dynamic system like the GSL.

[31] In addition, the nitrate stocks exhibit a strong interannual variability in the GSL related to winter convection [*Plourde and Therriault*, 2004] on which the magnitude of primary production is strongly dependent. In early spring, nitrate concentrations in the surface mixed layer were up to 5 mmol/m^3 lower in 1997 (7 mmol N/m^3) than during the CJGOFS's sampling years (9–12 mmol N/m^3 [*Plourde and Therriault*, 2004]). Figure 3 shows that the model reproduces nitrate concentrations (6.3–7.7 mmol N/m^3 in February-March) very close to the value given by *Plourde and Therriault* [2004] for the year 1997. This suggests that interannual variability can also contribute to explain the apparent discrepancy between our estimate of the mean annual production and the in situ estimate of *Roy et al.* [2000]. Our simulated GSL mean annual primary production is finally in the range of reported estimates for shelf seas at moderate to high latitudes, such as the Central North Sea (90–97 g C/m^2/yr [*Skogen and Moll*, 2000]), the Scotian Shelf (62–102 g C/m^2/yr [*Mousseau et al.*, 1996]), and the Black

Sea (101 g C/m^2/yr with a C/N ratio of 6.625 [*Grégoire and Beckers*, 2004]).

5. Conclusion

[32] Given the richness of the physical and biological conditions that are evidenced by the coupled model, it appears clearly that the Gulf of St. Lawrence cannot be considered as a single homogeneous entity. The strong variability that prevails in the GSL should be accounted for in the perspective of predicting and evaluating the effects of climate change on high-latitude marginal seas productivity. The spring bloom intensity being almost similar in all subregions of the GSL (Figure 6), the spatial variability of yearly integrated primary production (Figure 7) results from differences in summer primary production generated by different physical regimes. This suggests that, outside the spring bloom period, the primary production is locally of the same order of magnitude as during the spring bloom. Hence synoptic variability may be as important as the seasonal variability. The buoyancy-driven circulation in the NWG is influenced by the hydrographic and wind regimes [*Tang*, 1980; *Mertz et al.*, 1988, 1991; *Koutitonsky and Budgen*, 1991] and thus is subject to interannual variability. Upwelling events are linked to the synoptic wind variability which is typically 3–9 days in Eastern Canada [e.g., *Koutitonsky and Budgen*, 1991], but their frequency and duration may vary from year to year. Considering their impact on planktonic productivity at the subregional scale, the interannual variability of wind and hydrologic regimes can play a significant role in the interannual variability of the GSL planktonic production. This strengthens the need for an intensive monitoring program in the GSL like the Atlantic Zone Monitoring Program [*Therriault et al.*, 1998] which, in conjunction with the present model, will allow a better understanding of the interannual variability in the planktonic production. The present study highlights the abilities and limitations of the coupled model. The next step will be to run a refined version of the model for 1997 to 2003 to be analyzed with respect to the Atlantic Zone Monitoring Program database. Refinements would include a more accurate formulation of light conditions in estuarine waters, necessary to achieve a more realistic planktonic dynamics in the LSLE and western GSL, an improved formulation of nitrogen recycling in the whole water column and, finally, the use of year-specific seasonally varying boundary conditions of nitrate and Chl *a* at Cabot Strait and the Strait of Belle-Isle.

Appendix A: Planktonic Ecosystem Model Description

[33] All variables are expressed in units of mmol N/m^3, considering that nitrogen is the main limiting nutrient for phytoplankton growth. Silicate limitation is not considered in the model and is not expected to greatly influence the competition between both size fractions because the $Si/N0_3$ ratio is generally near 1/1 in the gulf waters [*Tremblay et al.*, 1997]. In the same way, phosphate was not found to limit phytoplankton growth [*Levasseur and Therriault*, 1987] and trace metals limitation is unlikely owing to their substantial concentrations in the coastal waters [*Yeats*, 1990]. In order to compare numerical solutions with historical data, primary production and phytoplankton biomass were converted into the usual units using a molar C/N ratio of 106/16 [*Redfield et al.*, 1963] and a C/chlorophyll *a* mass ratio of 55 [*Rivkin et al.*, 1996; *Sinclair*, 1978].

[34] The phytoplankton growth rate (μ) is a function of both light and nitrogen availability. It is computed following the Liebig's law of the minimum from nutrients-based ($dtn_{LP,SP}$) or light-based (dtc) doubling time of the biomass (equations A1–A3) [e.g., *Prieur and Legendre*, 1988; *Zakardjian and Prieur*, 1994, 1998; *Zakardjian et al.*, 2000]. The formulation is the same for the two size fractions of phytoplankton with parameters shown in Table 2. It gives for large phytoplankton:

$$\mu_{LP} = \frac{\ln(2)}{\max(dtn_{LP}, dtc)}, \tag{A1}$$

with

$$dtc = dtmin \cdot \left(1 + \frac{ke}{E}\right) \tag{A2}$$

$$dtn_{LP} = \frac{dtmin}{f(N)_{LP}}, \tag{A3}$$

where $f(N)_{LP}$ is the total nutrient uptake (described below) and dtmin is the minimum doubling time of the biomass. The same value of dtmin (0.5 day) is assigned in terms of carbon and nitrogen for both large and small phytoplankton to obtain light-based and nutrient-based maximum growth rates consistent with growth rate estimates in the GSL [e.g., *Tian et al.*, 2000; *Tamigneaux et al.*, 1997; *Sévigny et al.*, 1979]. The growth rate is set to 0 if one of the two doubling times exceeds 8.4 days [*Richardson et al.*, 1983]. Photosynthesis is described by a hyperbolic saturation curve [*Kiefer and Mitchell*, 1983] where E is the photosynthetically available radiation (PAR) experienced by phytoplankton. We assume that both phytoplankton size classes show the same response to light. The light field in the water column is computed through the classical Beer's law,

Surface z layer

$$E = 0.45 \cdot (1 - IC) \cdot SW \cdot \left[\exp^{-\left(k_w + k_p + k_{chla}\right) \cdot dz}\right] \tag{A4}$$

Subjacent z layers

$$E = E_{z-1} \cdot \left[\exp^{-\left(k_w + k_p + k_{chla}\right) \cdot dz}\right], \tag{A5}$$

with

$$k_{chla} = 0.0518 \cdot \left(CHLA^{-0.572}\right), \tag{A6}$$

where IC is the seasonal sea ice cover percentage and SW is the incident short wavelength irradiance at the sea surface used in the sea ice-ocean model. PAR representing about 40–50% of the total incoming radiation at the sea surface

[*Strickland*, 1958; *Morel*, 1988; *Kirk*, 1983], we assume the PAR to be 45% of SW. Pure seawater properties (k_w), terrigenous material (k_p), and phytoplankton self-shading (k_{chla}) attenuate the PAR through depth. The self-shading attenuation coefficient is calculated from Chl *a* concentration following Morel's formulation [*Morel*, 1988] (equations (A5)–(A6)). At this stage, freshwater-induced turbidity due to nonchlorophyllous matter, known to affect light conditions in the LSLE [e.g., *Sinclair*, 1978; *Nieke et al.*, 1997], is not considered. Hence k_p is set constant and adjusted to produce a maximum depth of the productive layer consistent with measured depths of the euphotic zone in the GSL (mostly 40–50 m [*Doyon et al.*, 2000]).

[35] The dissolved inorganic nitrogen uptake is computed using the substitutable model of *O'Neill et al.* [1989] for the two size classes of phytoplankton. It gives for large phytoplankton

$$f(N)_{LP} = \frac{k4_{LP} \cdot NO3 + k3_{LP} \cdot NH4}{k4_{LP} \cdot NO3 + k3_{LP} \cdot NH4 + k4_{LP} \cdot k3_{LP}}, \quad (A7)$$

$$NuNO3_{LP} = \frac{k4_{LP} \cdot NO3}{k4_{LP} \cdot NO3 + k3_{LP} \cdot NH4}, \quad (A8)$$

$$NuNH4_{LP} = \frac{k3_{LP} \cdot NH4}{k4_{LP} \cdot NO3 + k3_{LP} \cdot NH4}, \quad (A9)$$

where $NuNO3_{LP}$ and $NuNH4_{LP}$ are the nitrate and ammonium uptake fractions, respectively. No differences between both algae size classes were set for the nitrate uptake. Nonetheless, the ammonium is set to be the preferred inorganic nitrogen source [*Dorch*, 1990; *Levasseur et al.*, 1990] with a higher affinity for the small phytoplankton [*Tremblay et al.*, 2000]. This is expressed in the model by half-saturation constants for ammonium uptake significantly lower than for nitrate that, when used with the substitutable model of *O'Neill et al.* [1989], allow an inhibitory effect of ammonium on nitrate uptake as often observed [e.g., *Dorch*, 1990]. Phytoplankton losses include senescence, grazing, and sinking only for large algae. Senescence in phytoplankton being poorly quantified, we set it to 0.02 d^{-1} for both size classes.

[36] Formulations and parameters related to the mesozooplankton dynamics were chosen to reflect copepods since they widely dominate in abundance in the GSL [*de Lafontaine et al.*, 1991]. The grazing of the mesozooplankton is described by a modified Ivlev function [*Franks et al.*, 1986],

$$gz_{MEZ} = gmax_{MEZ} \cdot iv_{MEZ} \cdot (LP + MIZ) \cdot \left[1 - \exp^{-iv_{MEZ} \cdot (LP+MIZ)}\right]. \quad (A10)$$

In contrast to the classical Ivlev function, this formulation shows a non-saturating response of the grazing rate for high prey levels. Its use permits to dampen predator/prey oscillations [e.g., *Franks et al.*, 1986], and thus can provide stability to the planktonic ecosystem model forced by a highly changing physical environment. The mesozooplankton grazes on large phytoplankton and microzooplankton in the model, as it occurs in the GSL [*Ohman and Runge*, 1994], with a prey-specific grazing rate assumed to be proportional to the relative biomass of the prey. Because of their high variability ($gmax_{MEZ} = 0.16–1.5\ d^{-1}$ and $iv_{MEZ} = 0.1–2\ (mmol\ N/m^3)^{-1}$ [e.g., *Franks et al.*, 1986]), parameters of the grazing function were chosen to generate a peak of mesozooplankton biomass that follows the peak of large phytoplankton biomass with a time lag of about 2 weeks, i.e., half a generation time. Losses in mesozooplankton biomass are due to ammonium release, fecal pellets production (non-assimilated food), and mortality. Mortality is assumed to be mainly due to predation [e.g., *Eiane et al.*, 2002] and is described by a density-dependent quadratic function. As opposed to the linear form, the use of a quadratic function may limit the occurrence of oscillations generated in such non-linear systems [*Edwards and Brindley*, 1999; *Edwards and Yool*, 2000; *Edwards and Bees*, 2001]. The constant was set to 0.05 $(mmol\ N/m^3)^{-1}$ to produce mortality rates in the range of reported estimates [e.g., *Kiorbøe*, 1998; *Ohman et al.*, 2004].

[37] The grazing of the microzooplankton on small phytoplankton is formulated by a sigmoidal "Holling-type-III" function,

$$gz_{MIZ} = gmax_{MIZ} \cdot \left(\frac{SP^2}{SP^2 + k_{MIZ}^2}\right). \quad (A11)$$

This formulation provides a threshold-like limit for low biomass of prey which brings stability to the system [e.g., *Steele and Henderson*, 1992]. Its use is supported by the study of *Lancelot et al.* [1997] that evidenced that protozooplankton exerted a control on autotrophic flagellate biomass only beyond a certain threshold. The microzooplankton is known to be a major component of nitrogen recycling in marine systems [*Caron and Goldman*, 1990]. Following the study of *Riegman et al.* [1993], we set the fraction of food ingested by the microzooplankton and becoming biomass to 30%. *Lehrter et al.* [1999] reported that 26–27% of the total nitrogen release of microzooplankton can be in the dissolved organic form. Assuming a value of 30% in the model, it results that 21% of the food ingested is released as DON. The remaining 49% is lost as ammonium [e.g., *Anderson*, 1992]. Other loss terms of the microzooplankton component are senescence and grazing by the mesozooplankton. Similarly to phytoplankton, senescence was set to 0.02 d^{-1}.

[38] Fecal pellets and mesozooplankton and large phytoplankton mortality increase the PON concentration. The PON equation allows for its sedimentation and includes a fragmentation term into DON [e.g., *Gowing and Silver*, 1983; *Grossart and Ploug*, 2001]. The sinking material that leaves the last active layer in the model is assumed to be definitely trapped into the sediment. Finally, the ammonification of DON, considered here as the labile fraction, contributes to fuel the regenerated primary production [e.g., *Berman et al.*, 1999]. In the GSL, the dissolved organic carbon (DOC) remineralization rates have been reported to vary between 0.01 and 0.4 d^{-1} [*Packard et al.*, 2001]. Assuming a faster overturning of DON versus DOC, we set its decay rate to 0.4 d^{-1}.

[39] **Acknowledgments.** This work was supported by grants from the Natural Sciences and Engineering Research Council (BZ individual grant), the Canadian Foundation for Innovation, the Canadian Space Agency, and Fisheries and Oceans Canada. The technical contribution of J. Caveen and F. Roy, who helped to the development of the models and associated numerical and graphical tools, is gratefully acknowledged. The authors wish to acknowledge use of the Ferret Program (NOAA's Pacific Marine Environmental Laboratory) for analysis and graphics in this paper. We thank the two anonymous reviewers for improving this paper through their constructive reviews. This research is part of fulfillment of the requirements for a Ph.D. degree at the Université du Québec à Rimouski.

References

Anderson, T. R. (1992), Modelling the influence of food C:N ratio and respiration on growth and nitrogen excretion in marine zooplankton and bacteria, *J. Plankton. Res.*, *14*, 1645–1671.

Benoît, J., M. I. El-Sabh, and C. L. Tang (1985), Structure and seasonal characteristics of the Gaspe Current, *J. Geophys. Res.*, *90*, 3225–3236.

Berman, T., C. Bechemin, and S. Y. Maestrini (1999), Release of ammonium and urea form dissolved organic nitrogen in aquatic ecosystems, *Aquat. Microb. Ecol.*, *16*, 295–302.

Bourgault, D., and V. G. Koutitonsky (1999), Real time monitoring of the freshwater discharge at the head of the St. Lawrence Estuary, *Atmos. Ocean*, *37*, 203–220.

Caron, D. A., and J. C. Goldman (1990), Protozoan nutrient regeneration, in *Ecology of Marine Protozoa*, edited by G. M. Capriulo, pp. 203–306, Oxford Univ. Press, New York.

Claereboudt, M. R., J. Cote, J. C. Bonardelli, and J. H. Himmelman (1995), Seasonal variation in abundance and size structure of phytoplankton in Baie des Chaleurs, southwestern Gulf of St. Lawrence, in relation to physical oceanographic conditions, *Hydrobiologia*, *306*, 147–157.

Crise, A., J. I. Allen, J. Baretta, G. Crispi, R. Mosetti, and C. Solidoro (1999), The Mediterranean pelagic ecosystem response to physical forcing, *Prog. Oceanogr.*, *44*, 219–243.

Daly, K. L., D. W. R. Wallace, W. O. Smith Jr., A. Skoog, R. Lara, M. Gosselin, E. Falck, and P. L. Yager (1999), Non-Redfield carbon and nitrogen cycling in the Arctic: Effects of ecosystem structure and dynamics, *J. Geophys. Res.*, *104*, 3185–3199.

Dauchez, S., L. Legendre, L. Fortier, and M. Levasseur (1996), Nitrate uptake by size-fractionated phytoplankton on the Scotian Shelf (Northwest Atlantic): Spatial and temporal variability, *J. Plankton Res.*, *18*, 577–595.

de Lafontaine, Y., S. Demers, and J. A. Runge (1991), Pelagic food-web interactions and productivity in the Gulf of St. Lawrence: A perspective, in *The Gulf of St. Lawrence: Small Ocean or Big Estuary?*, edited by J.-C. Therriault, *Can. Spec. Publ. Fish. Aquat. Sci.*, *113*, pp. 99–123, Dep. of Fisheries and Oceans, Ottawa, Ont., Canada.

Demers, S., L. Legendre, and J.-C. Therriault (1986), Phytoplankton responses to vertical tidal mixing, in *Tidal Mixing and Plankton Dynamics, Lecture Notes Coastal Estuarine Stud.*, vol. 17, edited by J. Bowman, M. Yentsch, and W. T. Peterson, pp. 1–40, Springer, New York.

Dorch, Q. (1990), The interaction between ammonium and nitrate uptake in phytoplankton, *Mar. Ecol. Prog. Ser.*, *61*, 183–201.

Doyon, P., B. Klein, R. G. Ingram, L. Legendre, J.-É. Tremblay, and J.-C. Therriault (2000), Influence of wind mixing and upper layer stratification on phytoplankton biomass in the Gulf of St. Lawrence, *Deep Sea Res., Part II*, *47*, 519–545.

Dubinsky, Z., and I. Berman-Frank (2001), Uncoupling primary production from populations growth in photosynthesizing organisms in aquatic ecosystems, *Aquat. Sci.*, *63*, 4–17.

Ducklow, H. W., and M. J. R. Fasham (1992), Bacteria in the greenhouse: Modeling the role of oceanic plankton in the global carbon cycle, in *Environmental Microbiology*, edited by R. Mitchell, pp. 1–31, Wiley, Hoboken, N. J.

Edwards, A. M., and M. A. Bees (2001), Generic dynamics of a simple plankton population model with a non-integer exponent of closure, *Chaos Solitons Fractals*, *12*, 289–300.

Edwards, A. M., and J. Brindley (1999), Zooplankton mortality and the dynamical behaviour of plankton population models, *Bull. Math. Biol.*, *61*, 303–339.

Edwards, A. M., and A. Yool (2000), The role of higher predation in plankton population models, *J. Plankton Res.*, *22*, 1085–1112.

Eiane, K., D. L. Aksnes, M. D. Ohman, S. Wood, and M. B. Martinussen (2002), Stage-specific mortality of *Calanus* spp. under different predation regimes, *Limnol. Oceanogr.*, *47*, 636–645.

El-Sabh, M. I. (1976), Surface circulation patterns in the Gulf of St. Lawrence, *J. Fish. Res. Board Can.*, *33*, 124–138.

Engel, A., S. Goldthwait, U. Passow, and A. Alldredge (2002), Temporal decoupling of carbon and nitrogen dynamics in a mesocosm diatom bloom, *Limnol. Oceanogr.*, *47*, 753–761.

Fasham, M. J. R., H. W. Ducklow, and S. M. McKenzie (1990), A nitrogen-based model of plankton dynamics in the oceanic mixed layer, *J. Mar. Res.*, *48*, 591–639.

Flato, G. M. (1993), A particle-in-cell sea ice model, *Atmos. Ocean*, *31*, 339–358.

Fortier, L., M. E. Levasseur, R. Drolet, and J.-C. Therriault (1992), Export production and the distribution of fish larvae and their prey in a coastal jet frontal region, *Mar. Ecol. Prog. Ser.*, *85*, 203–218.

Franks, P. J. S. (2002), NPZ models of plankton dynamics: Their construction, coupling to physics, and application, *J. Oceanogr.*, *58*, 379–387.

Franks, P. J. S., J. S. Wroblewski, and G. R. Flierl (1986), Behaviour of a simple plankton model with food-level acclimation by herbivores, *Mar. Biol.*, *91*, 121–129.

Frost, B. W. (1972), Effects of size and concentration of food particles on the feeding behaviour of the marine planktonic copepod Calanus pacificus, *Limnol. Oceanogr.*, *17*, 805–815.

Fuentes-Yaco, C., P. Larouche, A. F. Vézina, C. Vigneau, and M. Gosselin (1995), Catalogue of phytoplankton pigment from the Gulf of St. Lawrence: Coastal Zone Color Scanner data from 1979 to 1980, *Can. Data Rep. Hydrogr. Ocean Sci.*, *135*, 91 pp.

Fuentes-Yaco, C., A. F. Vézina, M. Gosselin, Y. Gratton, and P. Larouche (1996), Influence of late-summer storms on the horizontal variability of phytoplankton pigment determined by Coastal Zone Color Scanner images in the Gulf of St. Lawrence, Canada, in *Ocean Optics XIII*, edited by S. G. Ackleson and R. Frouin, *Proc. SPIE Int. Soc. Opt. Eng.*, *2963*, 678–683.

Fuentes-Yaco, C., A. F. Vézina, P. Larouche, C. Vigneau, M. Gosselin, and M. Levasseur (1997a), Phytoplankton pigment in the Gulf of St. Lawrence, Canada, as determined by the Coastal Zone Color Scanner: Part 1. Spatio-temporal variability, *Cont. Shelf Res.*, *17*, 1421–1439.

Fuentes-Yaco, C., A. F. Vézina, P. Larouche, Y. Gratton, and M. Gosselin (1997b), Phytoplankton pigment in the Gulf of St. Lawrence, Canada, as determined by the Coastal Zone Color Scanner: Part 2, *Multivariate analysis, Cont. Shelf Res.*, *17*, 1441–1459.

Gilbert, D., and B. Pettigrew (1993), Current-meter data from Bonne-Bay, Newfoundland, during the summer of 1991, *Can. Data Rep. Hydrogr. Ocean Sci.*, *122*, 5 pp.

Gowing, M. M., and M. W. Silver (1983), Origins and microenvironments of bacteria mediating fecal pellet decomposition in the sea, *Mar. Biol.*, *73*, 7–16.

Gratton, Y., G. Mertz, and J. A. Gagné (1988), Satellite observations of tidal upwelling and mixing in the St. Lawrence Estuary, *J. Geophys. Res.*, *93*, 6947–6954.

Grégoire, M., and J. M. Beckers (2004), Modeling the nitrogen fluxes in the Black Sea using a 3D coupled hydrodynamical-biogeochemical model: Transport versus biogeochemical processes, exchanges across the shelf break and comparison of the shelf and deep sea ecodynamics, *Biogeosci. Disc.*, *1*, 107–166.

Greisman, P., and G. Ingram (1977), Nutrient distribution in the St. Lawrence Estuary, *J. Fish. Res. Board Can.*, *34*, 2117–2123.

Grossart, H.-P., and H. Ploug (2001), Microbial degradation of organic carbon and nitrogen on diatom aggregates, *Limnol. Oceanogr.*, *46*, 267–277.

Hargrave, B. T., G. C. Harding, K. F. Drinkwater, T. C. Lambert, and W. G. Harrison (1985), Dynamics of the pelagic food web in St. Georges Bay, southern Gulf of St. Lawrence, *Mar. Ecol. Prog. Ser.*, *20*, 221–240.

Hitchcock, G. L., and T. J. Smayda (1977), The importance of light in the initiation of the 1972–1973 winter-spring diatom bloom in Narragansett Bay, *Limnol. Oceanogr.*, *22*, 126–131.

Holland, M. M., and C. M. Bitz (2003), Polar amplification of climate change in coupled models, *Clim. Dyn.*, *21*, 221–232.

Holligan, P. M., W. M. Balch, and C. M. Yentsch (1984), The significance of subsurface chlorophyll, nitrite and ammonium maxima in relation to nitrogen for phytoplankton growth in stratified waters of the Gulf of Maine, *J. Mar. Res.*, *42*, 1051–1073.

Kiefer, D. A., and B. G. Mitchell (1983), A simple steady state description of phytoplankton growth based on absorption cross section and quantum efficiency, *Limnol. Oceanogr.*, *28*, 770–776.

Kiorbøe, T. (1998), Population regulation and role of mesozooplankton in shaping marine pelagic food webs, *Hydrobiologia*, *363*, 13–27.

Kiorbøe, T., F. Mohlenberg, and K. Hamburger (1985), Bioenergetics of the planktonic copepod *Acartia tonsa*: Relation between feeding, egg production and respiration, and composition of specific dynamic action, *Mar. Ecol. Prog. Ser.*, *26*, 85–97.

Kirk, J. T. O. (1983), *Light and Photosynthesis in Aquatic Ecosystems*, pp. 24–41, Cambridge Univ. Press, New York.

Koski, M., M. Viitasalo, and H. Kuosa (1999), Seasonal development of mesozooplankton biomass and production on the SW coast of Finland, *Ophelia*, *50*, 69–91.

Koutitonsky, V. G., and G. L. Budgen (1991), The physical oceanography of the Gulf of St. Lawrence: A review with emphasis on the synoptic variability of the motion, in *The Gulf of St. Lawrence: Small Ocean or Big Estuary?*, edited by J.-C. Therriault, *Can. Spec. Publ. Fish. Aquat. Sci.*, *113*, pp. 57–90, Dep. of Fisheries and Oceans, Ottawa, Ont., Canada.

Lancelot, C., S. Becquevort, P. Menon, S. Mathot, and J.-M. Dandois (1997), Ecological modelling of the planktonic microbial food-web, in *Belgian Research Program on the Antarctic, Scientific Results of Phase III (1992–1996): Marine Biogeochemistry and Ecodynamics*, vol. 1, edited by S. Caschetto, pp. 1–78, Fed. Off. for Sci., Tech. and Cult. Affairs, Brussels.

Lavoie, D., Y. Simard, and F. J. Saucier (2000), Aggregation and dispersion of krill at channel heads and shelf edges: The dynamics in the Saguenay-St. Lawrence Marine Park, *Can. J. Fish. Aquat. Sci.*, *57*, 1853–1869.

Legendre, L., and J. Le Fèvre (1995), Microbial food webs and the export of biogenic carbon in oceans, *Aquat. Microb. Ecol.*, *9*, 69–77.

Legendre, L., and J. Michaud (1998), Flux of biogenic carbon in oceans: Size-dependent regulation by pelagic food webs, *Mar. Ecol. Prog. Ser.*, *164*, 1–11.

Legendre, L., and F. Rassoulzadegan (1999), Stable versus unstable planktonic food webs in oceans, in *Microbial Biosystems: New Frontiers, Proceedings of the 8th International Symposium on Microbial Ecology*, edited by C. R. Bell, M. Brylinsky, and P. Johnson-Green, Atl. Can. Soc. For Microb. Ecol., Halifax, N. S., Canada.

Legendre, L., and R. B. Rivkin (2002), Fluxes of carbon in the upper oceans: Regulation by food-web control nodes, *Mar. Ecol. Prog. Ser.*, *242*, 95–109.

Lehrter, J. C., J. R. Pennock, and G. B. McManus (1999), Microzooplankton grazing and nitrogen excretion across a surface estuarine-coastal interface, *Estuaries*, *22*, 113–125.

Levasseur, M., and J.-C. Therriault (1987), Phytoplankton biomass and nutrient dynamics in a tidally induced upwelling: The role of the NO_3:-SiO_4 ratio, *Mar. Ecol. Prog. Ser.*, *39*, 87–97.

Levasseur, M., J.-C. Therriault, and L. Legendre (1984), Hierarchical control of phytoplankton succession by physical factors, *Mar. Ecol. Prog. Ser.*, *19*, 211–222.

Levasseur, M., P. J. Harrison, B. R. Heimdal, and J.-C. Therriault (1990), Simultaneous nitrogen and silicate deficiency of a phytoplankton community in a coastal jet-front, *Mar. Biol.*, *104*, 329–338.

Levasseur, M., L. Fortier, J.-C. Therriault, and P. J. Harrison (1992), Phytoplankton dynamics in a coastal jet frontal region, *Mar. Ecol. Prog. Ser.*, *86*, 283–295.

Levinsen, H., and T. G. Nielsen (2002), The trophic role of marine pelagic ciliates and heterotrophic dinoflagellates in Arctic and temperate coastal ecosystems: A cross-latitude comparison, *Limnol. Oceanogr.*, *47*, 427–439.

Lévy, M., P. Klein, and A.-M. Treguier (2001), Impact of sub-mesoscale physics on production and subduction of phytoplankton in an oligotrophic regime, *J. Mar. Res.*, *59*, 535–565.

Longhurst, A. R., and W. G. Harrison (1989), The biological pump: Profiles of plankton production and consumption in the upper ocean, *Prog. Oceanogr.*, *22*, 47–123.

Mahadevan, A., and D. Archer (2000), Modeling the impact of fronts and mesoscale circulation on nutrient supply and biogeochemistry of the upper ocean, *J. Geophys. Res.*, *105*, 1209–1225.

Mellor, G. L., and T. Yamada (1974), A hierarchy of turbulence closure models for planetary boundary layers, *J. Atmos. Sci.*, *31*, 1806–1971.

Mellor, G. L., and T. Yamada (1982), Development of a turbulence closure model for geophysical fluid problems, *Rev. Geophys.*, *20*, 851–875.

Mertz, G., M. I. El-Sabh, D. Proulx, and A. R. Condal (1988), Instability of a buoyancy-driven coastal jet: The Gaspé Current and its St. Lawrence precursor, *J. Geophys. Res.*, *93*, 6885–6894.

Mertz, G., V. G. Koutitonsky, and Y. Gratton (1991), On the seasonal cycle of the Gaspé Current, in *The Gulf of St. Lawrence: Small Ocean or Big Estuary?*, edited by J.-C. Therriault, *Can. Spec. Publ. Fish. Aquat. Sci.*, *113*, pp. 149–152, Dep. of Fisheries and Oceans, Ottawa, Ont., Canada.

Morel, A. (1988), Optical modeling of the upper ocean in relation to its biogenous matter content (case I waters), *J. Geophys. Res.*, *93*, 10,749–10,768.

Mousseau, L., L. Legendre, and L. Fortier (1996), Dynamics of size-fractionated phytoplankton and trophic pathways on the Scotian Shelf and at the shelf break, Northwest Atlantic, *Aquat. Microb. Ecol.*, *10*, 149–163.

Nieke, B., R. Reuter, R. Heuermann, H. Wang, M. Babin, and J.-C. Therriault (1997), Light absorption and fluorescence properties of chromophoric dissolved organic matter (CDOM) in the St. Lawrence Estuary (Case 2 waters), *Cont. Shelf Res.*, *17*, 235–252.

Ohman, M. D., and J. A. Runge (1994), Sustained fecundity when phytoplankton resources are in short supply: Omnivory by *Calanus finmarchicus* in the Gulf of St. Lawrence, *Limnol. Oceanogr.*, *39*, 21–36.

Ohman, M. D., K. Eiane, E. G. Durbin, J. A. Runge, and H.-J. Hirche (2004), A comparative study of *Calanus finmarchicus* mortality patterns at five localities in the North Atlantic, *ICES J. Mar. Sci.*, *61*, 687–697.

O'Neill, R. V., D. L. DeAngelis, J. J. Pastor, B. J. Jackson, and W. M. Post (1989), Multiple nutrient limitations in ecological models, *Ecol. Modell.*, *46*, 147–163.

Packard, T., et al. (2001), Dissolved organic carbon in the Gulf of St. Lawrence, *Deep Sea Res., Part II*, *47*, 435–459.

Parsons, T. R., M. Takahashi, and B. Hargrave (1984), *Biological Oceanographic Processes*, pp. 61–118, Elsevier, New York.

Peinert, R., and J.-C. Miquel (1994), The significance of frontal processes for vertical particle fluxes: A case study in the Alboran Sea (SW Mediterranean Sea), *J. Mar. Syst.*, *5*, 377–389.

Petrie, B., B. Toulany, and C. Garrett (1988), The transport of water, heat and salt through the Strait of Belle-Isle, *Atmos. Ocean*, *26*, 234–251.

Plourde, J., and J.-C. Therriault (2004), Climate variability and vertical advection of nitrate in the Gulf of St. Lawrence, Canada, *Mar. Ecol. Prog. Ser.*, *279*, 33–43.

Plourde, S., P. Joly, J. A. Runge, B. Zakardjian, and J. Dodson (2001), Life cycle of *Calanus finmarchicus* in the Lower St. Lawrence Estuary: The imprint of circulation and late timing of the spring phytoplankton bloom, *Can. J. Fish. Aquat. Sci.*, *58*, 647–658.

Pomeroy, L. R., and D. Deibel (1986), Temperature regulation of bacterial activity during the spring bloom in Newfoundland coastal waters, *Science*, *233*, 359–361.

Prieur, L., and L. Legendre (1988), Oceanographic criteria for new phytoplankton production, in *Toward a Theory on Biological-Physical Interactions in the World Ocean*, edited by B. J. Rothschild, pp. 71–112, Springer, New York.

Redfield, A. C., B. H. Ketchum, and F. A. Richards (1963), The influence of organisms on the composition of sea water, in *The Sea: Ideas and Observations on Progress in the Study of the Seas*, edited by M. N. Hill, pp. 26–27, Wiley-Intersci., Hoboken, N. J.

Ressler, P. H., and A. E. Jochens (2003), Hydrographic and acoustic evidence for enhanced plankton stocks in a small cyclone in the northeastern Gulf of Mexico, *Cont. Shelf Res.*, *23*, 41–61.

Richardson, K., J. Beardall, and J. A. Raven (1983), Adaptation of unicellular algae to irradiance: An analysis of strategies, *New Phytol.*, *9*, 157–191.

Riegman, R., B. R. Kuipers, A. A. M. Nooedeloos, and H. J. Witte (1993), Size-differential control of phytoplankton and the structure of plankton communities, *Neth. J. Sea Res.*, *31*, 255–265.

Rivkin, R. B., et al. (1996), Vertical flux of biogenic carbon in the ocean: Is there food web control?, *Science*, *272*, 1163–1166.

Rose, G. A., and W. C. Leggett (1988), Atmosphere-ocean coupling in the northern Gulf of St. Lawrence: Frequency-dependent wind-forced variations in nearshore sea temperatures and currents, *Can. J. Fish. Aquat. Sci.*, *45*, 1222–1233.

Roy, S., J.-P. Chanut, M. Gosselin, and T. Sime-Ngando (1996), Characterization of phytoplankton communities in the lower St. Lawrence Estuary using HPLC-detected pigments and cell microscopy, *Mar. Ecol. Prog. Ser.*, *142*, 55–73.

Roy, S., N. Silverberg, N. Romero, D. Deibel, B. Klein, C. Savenkoff, A. F. Vézina, J.-É. Tremblay, L. Legendre, and R. B. Rivkin (2000), Importance of mesozooplankton feeding for the downward flux of biogenic carbon in the Gulf of St. Lawrence (Canada), *Deep Sea Res., Part II*, *47*, 519–545.

Runge, J. A., and Y. de Lafontaine (1996), Characterization of the pelagic ecosystem in surface waters of the northern Gulf of St. Lawrence in early summer: The larval redfish-Calanus-microplankton interaction, *Fish. Oceanogr.*, *5*, 21–37.

Runge, J. A., M. Castonguay, Y. de Lafontaine, M. Ringuette, and J.-L. Beaulieu (1999), Covariation in climate, zooplankton biomass and mackerel recruitment in the southern Gulf of St Lawrence, *Fish. Oceanogr.*, *8*, 139–149.

Runge, J. A., P. J. S. Franks, W. C. Gentleman, B. A. Megrey, K. A. Rose, F. E. Werner, and B. A. Zakardjian (2005), Diagnosis and prediction in variability in secondary production and fish recruitment processes: Developments in physical-biological modeling, in *The Sea*, vol. 13, *The Global Coastal Ocean: Multi-Scale Interdisciplinary Processes*, edited by A. R. Robinson and K. Brink, Chap. 14, pp. 413–474, Harvard Univ. Press, Cambridge, Mass.

Saíz, E., and M. Alcaraz (1992), Enhanced excretion rates induced by small-scale turbulence in *Acartia* (Copepoda: Calanoida), *J. Plankton Res.*, *14*, 681–689.

Sambrotto, R. N., G. Savidge, C. Robinson, P. Boyd, T. Takahashi, D. M. Karl, C. Langdon, D. Chipman, J. Marra, and L. Codispoti (1993), Elevated consumption of carbon relative to nitrogen in the surface ocean, *Nature*, *363*, 248–250.

Saucier, F. J., and J. Chassé (2000), Tidal circulation and buoyancy effects in the St. Lawrence Estuary, *Atmos. Ocean*, *38*, 505–556.
Saucier, F. J., F. Roy, D. Gilbert, P. Pellerin, and H. Ritchie (2003), Modeling the formation and circulation processes of water masses and sea ice in the Gulf of St. Lawrence, Canada, *J. Geophys. Res.*, *108*(C8), 3269, doi:10.1029/2000JC000686.
Savenkoff, C., et al. (2000), Export of biogenic carbon and structure and dynamics of the pelagic food web in the Gulf of St. Lawrence: Part 1. Seasonal variations, *Deep Sea Res., Part II*, *47*, 585–607.
Savenkoff, C., A. F. Vézina, P. C. Smith, and G. Han (2001), Summer transports of nutrients in the Gulf of St. Lawrence estimated by inverse modelling, *Estuarine Coastal Shelf Sci.*, *52*, 565–587.
Semtner, A. J., Jr. (1976), A model for the thermodynamic growth of sea ice in numerical investigations of climate, *J. Phys. Oceanogr.*, *6*, 379–389.
Sévigny, J. M., M. Sinclair, M. I. El-Sabh, S. Poulet, and A. Coote (1979), Summer plankton distribution associated with the physical and nutrient properties on the northwestern Gulf of St. Lawrence, *J. Fish. Res. Board Can.*, *36*, 187–203.
Sheng, J. Y. (2001), Dynamics of a buoyancy-driven coastal-jet: The Gaspé Current, *J. Phys. Oceanogr.*, *31*, 3146–3162.
Simard, Y., and D. Lavoie (1999), The rich krill aggregation of the Saguenay–St. Lawrence Marine Park: Hydroacoustic and geostatistical biomass estimates, structure, variability, and significance for whales, *Can. J. Fish. Aquat. Sci.*, *56*, 1182–1197.
Sime-Ngando, T., M. Gosselin, S. Roy, and J.-P. Chanut (1995), Significance of planktonic ciliated protozoa in the Lower St. Lawrence Estuary: Comparison with bacterial, phytoplankton, and particulate organic carbon, *Mar. Ecol. Prog. Ser.*, *9*, 243–258.
Sinclair, M. (1978), Summer phytoplankton variability in the lower St. Lawrence estuary, *J. Fish. Res. Board Can.*, *35*, 1171–1185.
Skogen, M. D., and A. Moll (2000), Interannual variability of the North Sea primary production: Comparison from two model studies, *Cont. Shelf Res.*, *20*, 129–151.
Smayda, T. J. (1970), The suspension and sinking of phytoplankton in the sea, *Mar. Biol. Annu. Rev.*, *8*, 353–414.
Starr, M., and M. Harvey (2000), State of phytoplankton and zooplankton in the estuary and northwestern Gulf of St. Lawrence during 1999, *DFO Sci. Stock Status Rep. C4-18*, Can. Sci. Advis. Secr., Ottawa, Ont., Canada.
Starr, M., L. St-Amand, P. Joly, and J.-C. Therriault (2001), Variations spatio-temporelles du phytoplankton dans l'estuaire maritime du Saint-Laurent, *AZMP Bull.*, *1*, 21–23.
Steele, J. H., and E. W. Henderson (1992), The role of predation in plankton models, *J. Plankton Res.*, *14*, 157–172.
Steven, D. M. (1974), Primary and secondary primary production in the Gulf of St. Lawrence, *Mar. Sci. Cent. MS Rep. 26*, 116 pp., McGill Univ., Montreal, Quebec, Canada.
Strickland, J. D. H. (1958), Solar radiation penetrating the ocean: A review of the requirements, data and methods of measurement, with particular references to photosynthetic productivity, *J. Fish. Res. Bd. Can.*, *15*, 453–493.
Strom, S. L., M. A. Brainard, J. L. Holmes, and M. B. Olson (2001), Phytoplankton blooms are strongly impacted by microzooplankton grazing in coastal North Pacific waters, *Mar. Biol.*, *138*, 355–368.
Tamigneaux, E., M. Mingelbier, B. Klein, and L. Legendre (1997), Grazing by protists and seasonal changes in the size structure of protozooplankton and phytoplankton in a temperate nearshore environment (western Gulf of St. Lawrence, Canada), *Mar. Ecol. Prog. Ser.*, *146*, 231–247.
Tamigneaux, E., L. Legendre, B. Klein, and M. Mingelbier (1999), Seasonal dynamics and potential fate of size-fractionated phytoplankton in a temperate nearshore environment (Western Gulf of St. Lawrence, Canada), *Estuarine Coastal Shelf Sci.*, *48*, 253–269.
Tang, C. L. (1980), Mixing and circulation in the northwestern Gulf of St. Lawrence: A study of a buoyancy-driven current system, *J. Geophys. Res.*, *85*, 2787–2796.
Therriault, J.-C., and M. Levasseur (1985), Control of phytoplankton production in the St. Lawrence Estuary: Light and freshwater runoff, *Nat. Can.*, *112*, 77–96.
Therriault, J.-C., et al. (1998), Proposal for a Northwest Atlantic Zonal Monitoring Program, *Can. Tech. Rep. Hydrogr. Ocean Sci.*, *194*, 55 pp.
Thibault, D., R. Gaudy, and J. Le Fèvre (1994), Zooplankton biomass, feeding and metabolism in a geostrophic frontal area (Almeria-Oran Front, western Mediterranean): Significance to pelagic food webs, *J. Mar. Syst.*, *5*, 297–311.
Tian, R. C., et al. (2000), Effects of pelagic food-web interactions and nutrient remineralization on the biogeochemical cycling of carbon: A modeling approach, *Deep Sea Res., Part II*, *47*, 637–662.
Tian, R. C., A. F. Vézina, M. Starr, and F. J. Saucier (2001), Seasonal dynamics of coastal ecosystems and export production at high latitudes: A modeling study, *Limnol. Oceanogr.*, *46*, 1845–1859.
Tremblay, J.-É., L. Legendre, and J.-C. Therriault (1997), Size-fractionated effects of vertical stability on the biomass and production of phytoplankton in a large estuarine system, *Estuarine Coastal Shelf Sci.*, *45*, 415–431.
Tremblay, J.-É., L. Legendre, B. Klein, and J.-C. Therriault (2000), Size-differential uptake of nitrogen and carbon in a marginal sea (Gulf of St. Lawrence, Canada): Significance of diel periodicity and urea uptake, *Deep Sea Res., Part II*, *47*, 489–518.
Turner, J. T. (2002), Zooplankton fecal pellets, marine snow and sinking phytoplankton blooms, *Aquat. Microb. Ecol.*, *27*, 57–102.
Vandevelde, T., L. Legendre, J.-C. Therriault, S. Demers, and A. Bah (1987), Subsurface chlorophyll maximum and hydrodynamics of the water column, *J. Mar. Res.*, *45*, 377–396.
Wiggert, J., T. Dickey, and T. Granata (1994), The effect of temporal undersampling on primary production estimates, *J. Geophys. Res.*, *99*, 3361–3371.
Woods, J. (1988), Scale upwelling and primary production, in *Toward a Theory on Biological-Physical Interactions in the World Ocean*, edited by B. J. Rothschild, pp. 7–38, Springer, New York.
Yeats, P. A. (1990), Reactivity and transport of nutrients and metals in the St. Lawrence Estuary, in *Oceanography of a Large-Scale Estuarine System: The St. Lawrence, Coastal Estuarine Stud.*, vol. 39, edited by M. I. El-Sabh and N. Silverberg, pp. 155–165, Springer, New York.
Zakardjian, B., and L. Prieur (1994), A numerical study of primary production related to vertical turbulent diffusion with special reference to vertical motions of the phytoplankton cells in nutrient and light fields, *J. Mar. Syst.*, *5*, 267–295.
Zakardjian, B., and L. Prieur (1998), Biological and chemical signs of upward motions in permanent geostrophic fronts of the Western Mediterranean, *J. Geophys. Res.*, *103*, 27,849–27,866.
Zakardjian, B., Y. Gratton, and A. F. Vézina (2000), Late spring phytoplankton bloom in the Lower St. Lawrence Estuary: The flushing hypothesis revisited, *Mar. Ecol. Prog. Ser.*, *192*, 31–48.
Zakardjian, B., J. Sheng, J. A. Runge, I. McLaren, S. Plourde, K. R. Thompson, and Y. Gratton (2003), Effect of temperature and circulation on the population dynamics of *Calanus finmarchicus* in the Gulf of St. Lawrence and Scotian Shelf: Study with a coupled, three-dimensional hydrodynamic, stage-based life history model, *J. Geophys. Res.*, *108*(C11), 8016, doi:10.1029/2002JC001410.

V. Le Fouest, F. J. Saucier, and B. Zakardjian, Institut des Sciences de la Mer de Rimouski (ISMER), Université du Québec à Rimouski, 31o allee des Ursulines, Rimouski, Quebec G5L 3A1, Canada. (vincent_lefouest@uqar.qc.ca)
M. Starr, Fisheries and Oceans Canada, Maurice Lamontagne Institute, Mont-Joli, Quebec G1K 7Y7, Canada.